Anatomical, physiological and molecular properties of Martinotti cells in the somatosensory cortex of the juvenile rat

Yun Wang[1], Maria Toledo-Rodriguez[2,3], Anirudh Gupta[2,3], Caizhi Wu[4], Gilad Silberberg[2,3], Junyi Luo[4] and Henry Markram[2]

[1]*Division of Neurology Research, St. Elizabeth's Medical Center, Tufts University, Boston, MA 02135, USA*
[2]*Brain and Mind Institute, EPFL, Lausanne, 1015, Switzerland*
[3]*Department of Neurobiology, Weizmann Institute of Science, Rehovot 76100, Israel*
[4]*Cold Spring Harbour Laboratory, 1 Bungtown Road, Cold Spring Harbour, NY 11724, USA*

Whole-cell patch-clamp recordings followed by histochemical staining and single-cell RT-PCR were obtained from 180 Martinotti interneurones located in layers II to VI of the somatosensory cortex of Wistar rats (P13–P16) in order to examine their anatomical, electrophysiological and molecular properties. Martinotti cells (MCs) mostly displayed ovoid-shaped somata, bitufted dendritic morphologies, and axons with characteristic spiny boutons projecting to layer I and spreading horizontally across neighbouring columns more than 1 mm. Electron microscopic examination of MC boutons revealed that all synapses were symmetrical and most synapses (71%) were formed onto dendritic shafts. MCs were found to contact tuft, apical and basal dendrites in multiple neocortical layers: layer II/III MCs targeted mostly layer I and to a lesser degree layer II/III; layer IV MCs targeted mostly layer IV and to a lesser degree layer I; layer V and VI MCs targeted mostly layer IV and layer I and to a lesser degree the layer in which their somata was located. MCs typically displayed spike train accommodation (90%; $n = 127$) in response to depolarizing somatic current injections, but some displayed non-accommodating (8%) and a few displayed irregular spiking responses (2%). Some accommodating and irregular spiking MCs also responded initially with bursts (17%). Accommodating responses were found in all layers, non-accommodating mostly in upper layers and bursting mostly in layer V. Single-cell multiplex RT-PCR performed on 63 MCs located throughout layers II–VI, revealed that all MCs were somatostatin (SOM) positive, and negative for parvalbumin (PV) as well as vaso-active intestinal peptide (VIP). Calbindin (CB), calretinin (CR), neuropeptide Y (NPY) and cholecystokinin (CCK) were co- expressed with SOM in some MCs. Some layer-specific trends seem to exist. Finally, 24 accommodating MCs were examined for the expression of 26 ion channel genes. The ion channels with the highest expression in these MCs were (from highest to lowest); Caβ1, Kv3.3, HCN4, Caβ4, Kv3.2, Kv3.1, Kv2.1, HCN3, Caα1G, Kv3.4, Kv4.2, Kv1.1 and HCN2. In summary, this study provides the first detailed analysis of the anatomical, electro-physiological and molecular properties of Martinotti cells located in different neocortical layers. It is proposed that MCs are crucial interneurones for feedback inhibition in and between neocortical layers and columns.

(Resubmitted 5 August 2004; accepted after revision 24 August 2004; first published online 26 August 2004)
Corresponding author H. Markram: Brain and Mind Institute, EPFL, Lausanne, 1015 Switzerland.
Email: henry.markram@epfl.ch

The neocortex is vertically separated into six major layers that are specialized to receive input from the thalamus (layer IV and VI), provide feedback to the thalamus (layer VI) (Staiger *et al.* 1996), associate cortical activity (layer II/III), and generate the output (layer V). The manner in which activity between layers is co-ordinated in general, and which inhibitory feedback loops operate in particular, are still not well

Y. Wang and M. Toledo-Rodriguez contributed equally to this work.

DOI: 10.1113/jphysiol.2004.073353

understood. Horizontally, the neocortex is a continuous sheet of interconnected neurones, but the concept of 'elementary cortical units of operation' existing within this sheet was already introduced in the 1930's by Lorente de No (1938) and later strongly supported by Mountcastle's seminal work (Mountcastle, 1957). These functional neocortical modules (around 500 μm in diameter) are thought to be formed by a vertical column of collaborating neurones that respond to the same stimuli (Hubel & Wiesel, 1962; Tommerdahl *et al.* 1993). While there are typically no clear anatomical borders that correspond to functional ones, the diameter of functional columns is approximately the same as the horizontal spread of the axonal and dendritic arbours of pyramidal cells (PC) (300–500 μm) and of most neocortical neurones. This high density local interconnectivity provides up to 80% of the synapses onto neocortical neurones, but on its own does not explain functional borders since the horizontal spread of neurones is continuous. Topographical mapping onto the neocortex from the thalamus and between brain areas, may define 'centres' for functional columns, but competition between modules may still be required to form sharp borders. Lateral inhibition that extends beyond the dimensions of the local recurrent axonal network of PCs (300 μm) could mediate this competition and it is therefore important to understand the different sources of cross-columnar inhibition.

While some interneurones largely restrict their axons mostly to the layer in which the soma is located (small basket cells, neurogliaform cells, chandelier cells), many interneurones also extend their axons across multiple layers (large basket cells, Martinotti, bitufted, double bouquet, and bipolar cells) (Fairen *et al.* 1984). Very little is known, however, about the selectivity of interlayer targeting. Most interneurone types also restrict their axons to the dimensions of a cortical column with two major exceptions; large basket cells (LBCs) and Martinotti cells (MCs) (Fairen *et al.* 1984; Wang *et al.* 2002). LBCs typically provide long horizontal axons that cross multiple columns in the same layer that the soma is located, while MCs send their axons up to layer I to form an axonal arborization that crosses multiple columns in layer I to contact the distal tuft dendrites of pyramidal cells. Because of this distal dendritic innervation, the nature of MC-mediated inhibition is expected to differ substantially from that of LBCs.

The Martinotti cell was first reported by Carlo Martinotti in 1889 (Martinotti, 1889) and first named by Ramon y Cajal (Ramon y Cajal, 1891). This cell type, first found in layer V, was defined according to its ascending axonal collaterals reaching layer I where they ramify to form a fanlike spread of axonal collaterals (Fairen *et al.* 1984), with axons bearing spine-like boutons (Marin-Padilla, 1984). Subsequent studies revealed that MCs are present ubiquitously in different layers and areas of the neocortex as well as different ages and in many species. These include: mouse somatosensory (Lorente de No, 1922) and visual cortices (Valverde, 1976); rat visual (1, 3 and 4 months old; Ruiz-Marcos & Valverde, 1970), cingulate (1–2 months; Vogt & Peters, 1981) and frontal cortices (Kawaguchi & Kubota, 1998); the visual cortex of rabbit (Shkol'nik-Yarros, 1971), alticola (Hedlich & Werner, 1990), *microtus brandti* (Hilbig *et al.* 1991) and guinea-pig (Hedlich & Werner, 1986); several neocortical areas of *microtus agrestis,* hamster, hedgehog, the dwarf bat, dog, cow and sheep (Ferrer *et al.* 1986*a*,*b*); several neocortical areas in the mature cat (Marin-Padilla, 1972) including in the visual cortex (O'Leary, 1941); in the adult monkey pre-frontal cortex (Gabbott & Bacon, 1996); and also in human somatosensory (Ramon y Cajal, 1911), motor (Marin-Padilla, 1970) and visual cortices (Luth *et al.* 1994). The ubiquitous existence of MCs in the cerebral cortex of different ages and species suggests a central role in information processing in the cortical column. Indeed, MCs have been proposed to be involved in memory formation and storage (Eccles, 1983) and in neurodegenerative diseases (Beal *et al.* 1988).

Most previous studies on MCs have been limited to descriptions of their anatomical properties, largely based on Golgi staining, which may render only some neuronal processes visible (Ramon y Cajal, 1911; Marin-Padilla, 1970; Ferrer *et al.* 1986*a*,*b*). At the electrophysiological level, MCs have been reported to display 'regular' or 'burst' firing patterns to depolarizing somatic current injections (Kawaguchi & Kubota, 1997), which have also been reported to be low threshold interneurone (Kawaguchi, 1995). A more recent study has reported regenerative calcium activity in MCs which may be important in the bursting type of MCs (Goldberg *et al.* 2004). At the biochemical level, somatostatin (SOM) is reportedly expressed in MCs (Wahle, 1993; Kawaguchi & Kubota, 1996), while other biochemical markers, including neuropeptide Y (NPY) (Beal *et al.* 1988; Kuljis & Rakic, 1989; Obst & Wahle, 1995) and calbindin (CB) have also tested positive in MCs (Conde *et al.* 1994; Kawaguchi & Kubota, 1996; Kawaguchi & Kubota, 1997).

A systematic multidimensional study of the detailed anatomical, physiological and molecular properties of MCs is, however, still lacking. In particular, at the anatomical level, the presence of MCs in different layers is not well established, the morphological similarities and differences between MCs in different layers is not known, the cross-layer and cross-columnar axon targeting principles of MCs has not been isolated, the dendritic expanse of different MCs has not been determined, and the different shapes of MC somata are not clear. At the electrical level, the number of different response types and their frequencies of occurrence, as well as the heterogeneity of detailed electrical parameters, have not

been determined. The ion channel genes supporting MC electrical properties are also not known. At the biochemical level, the co-expression profiles for neuropeptide and calcium binding protein genes are not known.

In the present study, we employed whole-cell patch-clamp recordings to acquire electrophysiological properties, histochemical staining to obtain 3-D anatomical reconstructions and morphometric analyses, as well as aspiration of the cytoplasm to determine the mRNA expression profile of neurones using multiplex RT-PCR (Fig. 1). We report for the first time that (a) MCs are found in all layers II–VI, (b) they all display some common anatomical, electrophysiological and biochemical properties, (c) they display distinct layer-specific differences, and (d) infragranular MCs also target layer IV in addition to layer I. We also report for the first time, the ion channel genes expressed in MCs.

Methods

Slice preparation

All experimental procedures were carried out according to the Swiss federation rules for animal experiments. Wistar rats (13- to 16-days-old) were rapidly decapitated and neocortical slices (sagittal; 300 μm thick) were sectioned on a vibratome (DSK, Microslicer, Japan) filled with iced extracellular solution (composition below). Optimal slices (2–3 per hemisphere), running parallel to apical dendrites of PCs, were selected for recording. Slices were incubated for 30 min at 34°C and then at room temperature (24–25°C) until transferred to the recording chamber (34 or 24–25°C). The extracellular solution contained (mM): 125 NaCl, 2.5 KCl, 25 glucose, 25 $NaHCO_3$, 1.25 NaH_2PO_4, 2 $CaCl_2$ and 1 $MgCl_2$. Neurones in somatosensory cortex were identified using IR-DIC microscopy, with an upright microscope (Zeiss Axioplan, fitted with 40 × W/0.75 NA objective, Zeiss,

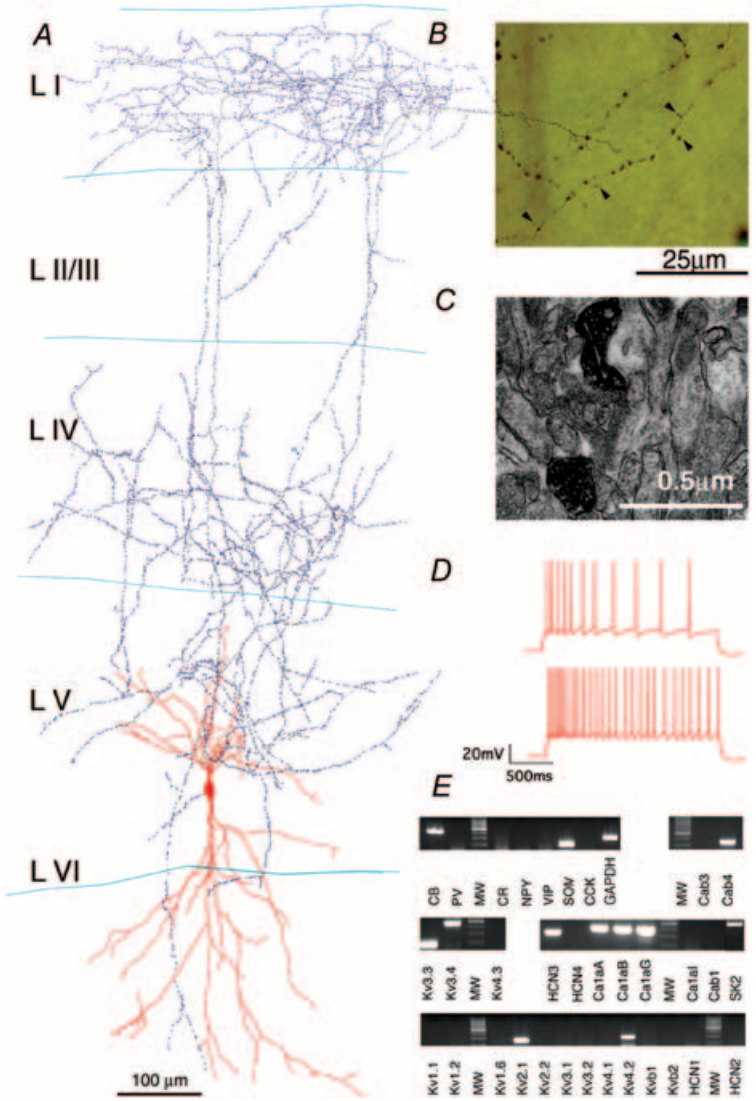

Figure 1. Features of a layer V MC
A, 3-D computer reconstruction (soma and dendrites are in red, axon in blue, boutons marked with dots). Note bitufted morphology, ovoid somata, axon targeting layers I, IV and V and downward dendritic projections. *B*, photo of spiny boutons on MC axons (arrows). *C*, EM image of MC boutons in layer I. *D*, classical accommodating discharge to sustained somatic current injections. *E*, single-cell RT-PCR results: agarose gel showing the expression of mRNAs encoding for the CaBPs (calbindin, CB; parvalbumin, PV; and calretinin, CR); the neuropeptides (neuropeptide Y, NPY; vasoactive intestinal peptide, VIP; somatostatin, SOM; cholecystokinin, CCK); the voltage-activated K^+ channels (Kv1.1, Kv1.2, Kv1.4, Kv1.6, Kv2.1, Kv2.2, Kv3.1, Kv3.2, Kv3.3, Kv3.4, Kv4.2 and Kv4.3) and their auxiliary subunits (Kvβ1 and Kvβ2); the K^+/Na^+ permeable hyperpolarization-activated ion channels (HCN1, HCN2, HCN3 and HCN4); the Ca^{2+}-activated K^+ channel (SK2); the voltage-activated calcium channels (Caα1A, Caα1B, Caα1G and Caα1I) and their auxiliary subunits (Caβ1, Caβ3 and Caβ4) and the ubiquitous protein GAPDH. See Table 1 for the lists of the primer pairs included into the different multiplexes, the name and accession number of the genes amplified and the length of the PCR product.

Oberkochen, Germany). Recorded neurones were selected up to 120 μm below the surface of the slice and laterally separated by up to 150 μm.

Electrophysiological recording

Somatic whole-cell recordings (pipette resistance 6–12 MΩ when there was no cytoplasm harvesting or 1–3 MΩ for recordings where the cytoplasm was harvested) were made and signals were amplified using either Axoclamp 2B or Axopatch 200B amplifiers (Axon Instruments). Neurones were submitted to a series of somatic current injection protocols, during whole-cell patch-clamp recordings, designed to capture their key active and passive electrical properties (Fig. 6). We focused on the shape of the first two action potentials (APs) generated just above threshold (AP Waveform), the change in the AP amplitude with time (AP Drop) and the membrane time constant for brief hyperpolarizing current pulses (Delta), the neuronal response to ramp current injection (AP Threshold), the sag, overshoot and rebound spike produced by different hyperpolarization current pulses of increasing magnitude (Sag), discharge responses to step current pulses of increasing magnitude (ID Rest), the subthreshold current–voltage relationship (I–V), the hyperpolarization after a burst of APs (s-AHP), the discharge responses to step current pulses around threshold (ID Thresh). A numerical breakdown of the electrical behaviour was obtained by measuring various aspects of the voltage responses to these stimulation protocols (Tables 4–7). Recordings were sampled at intervals of 10–400 μs using Igor (Wavemetrics, Lake Oswego, OR, USA), digitized by either an ITC-16 or ITC-18 interface (Instrutech, Great Neck, NY, USA) and stored on the hard disk of a Macintosh computer for off-line analysis (Igor). Voltages were recorded with pipettes containing (mM): 100 potassium gluconate, 20 KCl, 4 ATP-Mg, 10 phosphocreatine, 0.3 GTP, 10 Hepes (pH 7.3, 310 mOsm, adjusted with sucrose) and 0.5% biocytin (Sigma). Neurones were filled with biocytin by diffusion during the 30–90 min recordings. Membrane potentials were not corrected for the junction potentials between pipette and bath solution (∼9 mV).

Analysis of electrophysiological recordings

Most signals were sampled at 4 kHz, except for single action potentials (up to 20 kHz) and low-pass pre-filtered by 1 kHz (4–8 pole Bessel). Intrinsic properties: input resistances were approximated by linear regression of voltage deflections (± 15 mV from resting potential, –70 ± 2 mV) in response to 2 s current steps of four to eight different amplitudes after reaching steady state (end 200 ms of a 1 s current pulse). Steady-state current–voltage relationships were linear for most interneurones, allowing for this analysis. Membrane time constants were determined by fitting the decay phases of depolarizing and hyperpolarizing pulses (1 ms duration; voltage deflections of < 10 mV) to an exponential function, or by fitting the rising phases of the voltage traces used for determining the input resistances to an exponential function. Single AP analysis was performed on the first AP elicited by near-threshold depolarizations. Peak values of the AP and the fast AHP (fAHP) were determined by averaging 5–10 values around the peak. Maximum rise and fall rates were obtained as peak values after differentiating the 1st or 2nd AP. Classification of discharge behaviours was done according to previous studies (Gupta *et al.* 2000; Toledo-Rodriguez *et al.* 2003). Neurones were classified according to both their initial and steady-state discharge responses to step current injections. The initial response could be an onset delay ('d'), typically several hundred milliseconds before initiation, a burst onset ('b'), in which a group of two to five high frequency APs preceded the steady-state response, or an onset that was neither a delay nor a burst, which is referred to as a classical onset response ('c'). The steady-state discharge pattern was divided into accommodating ('AC'), non-accommodating ('NAC') and irregular spiking ('IS') responses. Accommodating discharge was characterized by a monotonic decrease in discharge rate throughout the duration of the current step injection while non-accommodating cells displayed little (less than ±10%) fluctuation in their instantaneous discharge frequency throughout the response. The degree of accommodation was quantified according to the ratio between the initial five ISIs and the latest five ISIs in the discharge response. Irregular spiking discharge behaviour was characterized by irregular discharges of APs. Discharge behaviours were robust up to 4 × threshold current injections (30–300 pA, depending on the individual neuronal input resistance) and stable for different holding potentials (from −85 to −60 mV) as well as different temperatures (20–24 and ∼34°C).

Histological procedures

After recording, slices were fixed for 24 h in cold 0.1 M phosphate buffer (PB, pH 7.4) containing 2% paraformaldehyde, 1% glutaraldehyde and 0.3% saturated picric acid. Thereafter, slices were rinsed several times (10 min each) in PB. To block endogenous peroxidases, slices were transferred into phosphate buffer containing 3% H_2O_2 for 30 min. After five to six rinses in PB (10 min each), slices were incubated overnight at 4°C in biotinylated horseradish peroxidase conjugated to avidin according to the manufacturer's protocol (ABC-Elite, Vector Laboratories, Peterborough, UK): 2% A, 2% B and 1% Triton X-100. Following incubation, sections were washed several times in PB and developed with diaminobenzidine (DAB, 0.14%) under visual control

using a bright-field microscope (Zeiss Axioskop) until all processes of the cells appeared clearly visible (usually after 2–4 min). The reaction was stopped by transferring the sections into PB. After washing in the same buffer, slices were mounted in aqueous mounting medium (IMMCO Diagnostics, Inc). In some cases, slices were re-sectioned into 100 μm thick sections before mounting. Staining of slices for EM examination was performed as described in Wang *et al.* (2002); the histochemical staining procedure was the same as mentioned above except for one step where the slices were quickly frozen with liquid N_2 instead of using Triton X-100. After the histochemical staining, the slices in which the filled cells were well visualized were re-sectioned at 100 μm thickness. To enhance the staining contrast, slices were postfixed for 45 min in 1% phosphate-buffered osmium tetroxide (Merck) and counterstained in 1% uranyl acetate. After several rinses in PB, sections were flattened between two glass slides and dehydrated through an ascending series of ethanol in small glass vials for 15 min each. Following two 10 min washes in propylene oxide (Merck), slices were embedded in Epon resin overnight at room temperature (Durcupan, Fluka, Buchs, Switzerland); afterwards slices were flat-embedded in Epon resin between a coated glass slide and a cover slip. Subsequently, light microscopic observation and 3-D reconstruction of the cells were carried out. Later some areas rich with interneurone boutons were re-embedded for cutting serial ultrathin sections, which were finally examined with electron microscopy (EM).

3-D computer reconstruction

3-D neurone models were reconstructed from stained cells using the Neurolucida system (MicroBrightField Inc., USA) and a bright-field light microscope (Olympus). After the staining procedure, there is ~25% shrinkage of the slice thickness and ~10% anisotropic shrinkage along the *X*- and *Y*-axes. Only shrinkage of thickness was corrected.

Quantitative morphometry (morphological analysis)

Reconstructed neurones were quantitatively analysed with NeuroExplorer (MicroBrightField Inc., USA). An array of eight axonal, and six dendritic parameters, designated as the 'morphology profile' (m-profile), was obtained to quantitatively compare the axonal and dendritic arbours of the Martinotti cells. An example of a layer V MC is given in Fig. 2. The axonal parameters include (Fig. 2*A* and *B*): (1) axonal Sholl distance (ASD), defined as the number of axonal intersections as a function of distance from the soma. A series of Sholl circles with 20 μm stepped radii centred in the interneurone soma were delineated and the number of axonal intersections in each stepped region and their distances to the centre were calculated. The maximum radius of Sholl circles used for the ASD calculation was 1 mm; (2) axonal segment lengths (ASL), defined as the length of axonal segments between two branch points or between a branch point and an end point; (3) axonal branch order (ABO), the branching frequency of an interneurone axon tree; (4) bouton density (BD), calculated as the number of boutons per axon length; (5) maximum axonal branch angle (MABA), the maximum angle formed between the extending distal line of the parent axonal segment and child axonal segments. Although the MABAs vary from less than 10 deg to nearly 180 deg, most MABAs lie between 40 and 100 deg; (6) planar axonal branching angle (PABA), the angle formed between the extending distal line of the parent axonal segment and a child axonal segment; (7) total number of axonal segments (SEG); (8) total number of boutons per cell (BT). Dendritic parameters were obtained by applying the same criteria as for the axonal structure and designated (Fig. 2*A* and *C*): (1) dendritic Sholl distance (DSD); (2) dendritic segment length (DSL); (3) dendritic branch order (DBO); (4) maximum dendritic branch angle (MDBA); and (5) planar dendritic branch angle (PDBA), respectively. In addition, the average length of the dendritic tree (ALDT) was defined as the average length of a single dendrite including all its branches (dendritic tree).

EM examination

In order to determine the postsynaptic targets of a filled MC, a region containing boutons only belonging to the studied MC was selected. The targets of all the boutons encountered in subsequent serial sections were examined under EM according to established criteria (Peters *et al.* 1991). Briefly, a postsynaptic target of a filled bouton was judged to belong to soma/dendrite/spine, based on its ultrastructural characteristics. Identification of the nature of postsynaptic dendritic shafts (pyramidal *versus* interneurone) was according to the previously published criteria (Peters *et al.* 1991). Briefly, dendritic shafts of a presumed PC have less cell organs presenting light cytoplasm and the dendritic shafts of a presumed interneurone have more cell organs presenting darker cytoplasm. When the plane of the section was not perpendicular to the junction of membranes, the synaptic cleft was revealed by tilting the section using the goniometer of the EM.

Cytoplasm harvesting and single-cell reverse transcription

This was performed as previously described (Cauli *et al.* 1997; Wang *et al.* 2002). In brief, recording pipettes were loaded with 5 μl of RNAse-free intracellular solution. At the end of the recording, cell cytoplasm was aspirated into the recording pipette under visual control by applying gentle negative pressure. Only cells in which the seal was intact throughout the recording, and whose nucleus was

not harvested, were further processed. The electrode was then withdrawn from the cell to form an outside-out patch that prevented contamination as the pipette was removed. The tip of the pipette was broken and the contents of the pipette expelled into a test tube by applying positive pressure. mRNA was reverse transcribed using an oligo-dT primer (25 ng μl^{-1}) and 100 Units of Superscript II reverse transcriptase (Gibco, BRL) in a final volume of 20 μl. After 50 min incubation at 42°C, the cDNA was frozen and stored at −20°C before further processing.

Multiplex PCR

Multiplex PCR conditions were optimized using total RNA purified from rat neocortex, so that a PCR product could be detected from 0.25–1 ng of total RNA without contamination caused by non-specific amplification. For the list of primer pairs included into the different multiplexes, the name and accession number of the genes amplified and the length of the PCR product see Table 1. Three different multiplex PCR reactions were performed for testing the expression of 30 mRNA

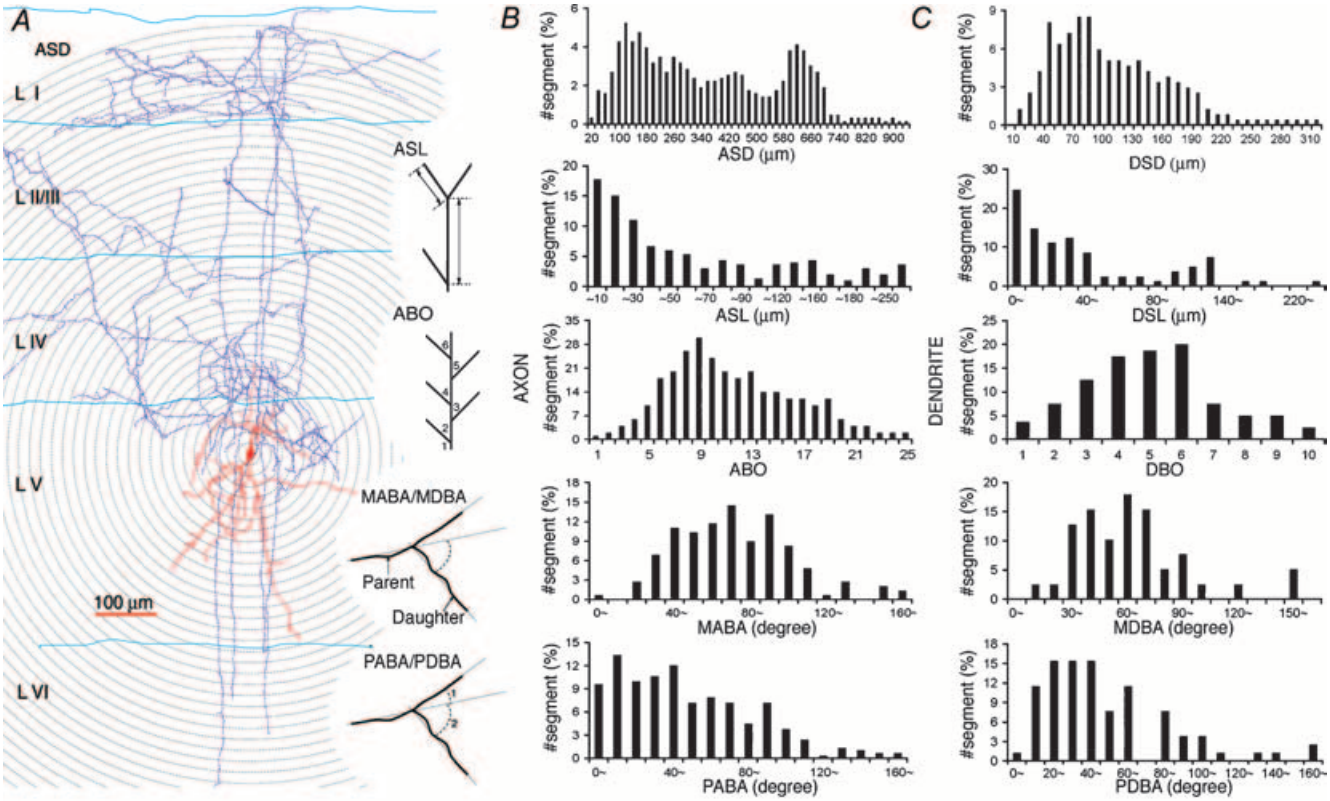

Figure 2. Morphometric analysis of a layer V MC
A, diagram of a reconstructed neurone and demonstration of its morphometric parameters (soma and dendrites in red, axon in blue). ASD, axon Sholl distance. Serial Sholl circles with 20 μm-stepped radii were centred in the soma. Numbers of intersections within each Sholl circle were counted and graphed as a function of distance to the centre. ASL, axonal segment length; defined as the length of axonal segment between two neighbouring branch points or between a branch point and an end point. ABO, axonal branch order; represents the frequency of axonal branching, its increases after each branch point from the initial axon segment. MABA or MDBA, maximum axonal or dendritic branch angle; the maximum angle formed between the extending distal line of a parent axonal segment and the daughter axonal segments (the lower bigger angle marked with a dash arc). PABA or PDBA, planar axonal or dendritic branching angle; the maximum angle formed between the extending distal line of the parent axonal segment and a daughter axonal segment (two planar angles were formed after branching). *B*, histograms of five major axonal parameters (for the layer V MC in *A*). The ASD histogram shows a first peak due to the axonal cluster formed in layer IV, and a second peak about 600–700 μm away due to the dense axonal cluster in layer I. The ASL histogram presents the different lengths of axonal segments. The ABO histogram presents distributions of axonal segment distribution in terms of branch orders. Most segments are 6–19th branch order. The MABA histogram shows the axonal segment distribution of this MC. The MABAs vary from less than 10 deg to nearly 180 deg, but most MABAs are arranged between 40 and 100 deg. The PABA histogram at the bottom shows the axonal segment distribution plotted according to planar axonal branch angles. *C*, histograms of five major dendritic parameters (for the layer V MC in *A*) as before for axons.

species from each cell. The genes co-amplified in each of three multiplex–PCR reactions were Pool I (CB, PV, CR and GAPDH), Pool II (Kv1.1, Kv1.2, Kv1.6, Kv2.1, Kv2.2, Kv3.1, Kv3.2, Kv4.2, Kvβ1, Kvβ2, HCN1 and HCN2), Pool III (Kv1.4, Kv3.3, Kv3.4, Kv4.3, HCN3, HCN4, Caα1A, Caα1B, Caα1G, Caα1I, Caβ1, Caβ3, Caβ4 and SK2). Pool 1 was already calibrated to give PCR products for each gene with even intensity (Wang *et al.* 2002). Pools II and III were calibrated to give PCR products for each gene with even intensity starting from 1 ng of brain total mRNA. During calibration, different combinations of genes were distributed between the two pools (II and III) and different primer pairs were tested until an even amplification of all genes in the pool was obtained.

The first amplification round consisted of 10 min hot start at 95°C followed by 25 cycles (94°C for 40 s, 56°C (pool I and II) or 58°C (pool III) for 40 s and 72°C for 1 min) performed with a programmable thermocycler (Eppendorf, Germany). For each pool all genes were simultaneously amplified in a single tube containing 1/10 (pool I) or 2/5 (pools II and III) of the RT product, 100 nM of each of the primers, 200 μM of each dNTP (Promega), 1 M betaine (Sigma) and 5 U of HotStarTaq DNA polymerase (Qiagen, Hilden, Germany) in a final volume of 100 μl. A second round of PCR consisted of 40 cycles (94°C for 40 s, 56°C (pool I and II) or 58°C (pool III) for 40 s and 72°C for 1 min) was performed. In this case, each gene was individually amplified in a separate test tube containing: 1 μM of its specific primers, 2 μl of the 1st PCR product (template), 200 μM of each dNTP, 1 M betaine and 1 U of TaqZol DNA polymerase (Tal-Ron Ltd, Israel), in a final volume of 20 μl. The products of the 2nd PCR were analysed in 1.5% agarose gels using ethidium bromide. Amplification specificity was randomly verified by restriction analysis.

Controls for the RT-PCR

For each PCR amplification, controls for contaminating artefacts were performed using sterile water instead of cDNA. A control for non-specific harvesting of surrounding tissue components was randomly employed by advancing pipettes into the slice and retrieving without seal formation and suction. Both types of controls gave negative results throughout the study. Amplification of genomic DNA could be excluded by the intron-overspanning location of many of the primers and by the fact that the cell nucleus was never harvested. Moreover controls in which the RT was omitted gave negative results.

Statistical analysis

Student's *t* tests were applied to compare between two groups of quantitative parameter values. Data are given as means ± standard deviation (S.D.) or means ± standard error (S.E.M.).

Results

Morphological criteria for Martinotti cells

Martinotti cells were readily distinguished from other interneurones mainly according to their axonal arborization. The essential criteria were: (a) axonal projections with a horizontal spread in layer I that typically extended beyond a column radius (150 μm) (see Fig. 1*A*), and (b) axonal collaterals decorated with spiny boutons (Fig. 1*C*). Additionally, MCs often presented more spines on their dendrites than other types of interneurones at this stage of development. One hundred and eighty MCs were anatomically verified according to the two essential axonal criteria throughout layers II–VI (layer II/III, $n = 62$; layer IV, $n = 52$, layer V, $n = 51$, layer VI, $n = 15$). Of these neurones, 91 with high quality axonal staining (27 in layer II/III, 28 in layer IV, 29 in layer V and 7 in layer VI) and 77 with high quality dendritic staining (22 in layer II/III, 20 in layer IV, 26 in layer V and 9 in layer VI) were examined at the light microscopic (LM) level for cross-layer comparisons, and 24 (10 in layer II/III, 7 in layer IV, 6 in layer V and 1 in layer VI) were randomly selected and 3-D computer-reconstructed in order to perform a quantitative comparison of MCs located in different layers.

Morphological characteristics

Most MC somata were ovoid or spindle shaped (94%), whereas others could have a pyramidal, round or multipolar form. MC somata usually gave rise to vertically orientated bundles of two to four primary dendrites from opposite somatic poles (bitufted dendritic morphology, 89%), with one of the primary dendrites branching more frequently and descending to deeper layers (72%, Fig. 3). Typically, MC dendrites were beaded (96%) and bore spines with sparse to medium density (86%). MC dendrites often branched frequently giving rise to the most elaborate dendritic trees of all the interneurones at this stage of neocortical development (DBO in Table 2). The lateral expanse of the dendritic arborization was usually less than that of the basal dendritic arbour of PCs (~300 μm of diameter) (Table 2), suggesting that MCs receive input signals from several layers, but within the dimensions of a cortical column.

MC axons often emerged from the 1st or 2nd branch order of a dendrite (81%) and in a few cases (8%), especially in infragranular layers, axons emerged from 3rd or higher dendritic branch orders. The remainder (11%) directly sent axons out from their somata. Axons projected towards the pia where they formed a cluster in layer I from where long horizontal collaterals emerged spreading

Table 1. PCR primers used

Gene	GenBank Accession no		Primers (from 5′ to 3′)	Fragment size (bp)
CB[1]	M27839	sense	AGGCACGAAAGAAGGCTGGAT	432
		antisense	TCCCACACATTTTGATTCCCTG	
PV[1]	M12725	sense	AAGAGTGCGGATGATGTGAAGA	389
		antisense	ATTGTTTCTCCAGCATTTTCCAG	
CR[1]	X66974	sense	CTGGAGAAGGCAAGGAAAGGT	311
		antisense	AGGTTCATCATAGGGACGGTTG	
NPY[1]	M15880	sense	GCCCAGAGCAGAGCACCC	362
		antisense	CAAGTTTCATTTCCCATCACCA	
VIP[1]	X02341	sense	TGCCTTAGCGGAGAATGACA	290
		antisense	CCTCACTGCTCCTCTTCCCA	
SOM[1]	K02248	sense	ATCGTCCTGGCTTTGGGC	208
		antisense	GCCTCATCTCGTCCTGCTCA	
CCK[1]	K01259	sense	CGCACTGCTAGCCCGATACA	216
		antisense	TTTCTCATTCCGCCTCCTCC	
GAPDH[2]	M17701	sense	GCCATCAACGACCCCTTCAT	315
		antisense	TTCACACCCATCACAAACAT	
Kv1.1[2]	M26161	sense	CCGCCGCAGCTCCTCTACT	209
		antisense	CAAGGGTTTTGTTTGGGGGCTTTT	
Kv1.2[2]	X16003	sense	GAAAAGTAGAAGTGCCTCTACCATAA	458
		antisense	TTGATATGGTGTGGGGGCTATGA	
Kv1.4[2]	X16002	sense	CTGGGGGACAAGTCAGAGTATCTA	434
		antisense	ACTCTCCTCGGGACCACCT	
Kv1.6	X17621	sense	GGGAACGGCGGTCCAGCTA	351
		antisense	GTGCATCTCATTCACGTGACTGAT	
Kv2.1[2]	X16476	sense	CAACTTCGAGGCGGGAGTC	229
		antisense	TCCAGTCAACCCTTCTGAGGAGTA	
Kv2.2[2]	M77482	sense	ACCAGGAGGTTAGCCAAAAAGACT	446
		antisense	AGGCCCCTTATCTCTGCTTAGTGT	
Kv3.1[2]	X62840	sense	CCAACAAGGTGGAGTTCATCAAG	640
		antisense	TGGTGTGGAGAGTTTACGACAGATT	
Kv3.2[2]	X62839	sense	ACCTAATGATCCCTCAGCGAGTGA	302
		antisense	CAAAATGTAGGTGAGCTTGCCAGAG	
Kv3.3	M84211	sense	GAGACCCCCGTCCCAATG	179
		antisense	CGGGGGAAGGGGCATAGTC	
Kv3.4[2]	X62841	sense	TCAGGCACACGGGACAGAAAC	418/522
		antisense	GGGCAGAGGACTTGGGAGACATA	
Kv4.2[2]	S64320	sense	CCGAATCCCAAATGCCAATGTG	265
		antisense	CCTGACGATGTTTCCTCCCGAATA	
Kv4.3	U42975	sense	GGGCAAGACCACGTCACTCA	296/386
		antisense	CTGCCCTGGATGTGGATGGT	
Kvb1[2]	X70662	sense	AAGGGAGAAAACAGCAAAACAAGC	170
		antisense	TGGCACCAAGGTTTTCAATGAGTT	
Kvb2	X76724	sense	ACAGTGGCATCCCACCCTACT	283
		antisense	GTGGACGATGGAGGACGACAAT	
HCN1	AF247450	sense	CCTCAAATGACAGCCCTGAATTG	405
		antisense	TCGGTGTGGAACTACCAGGTGT	
HCN2	AF247451	sense	CTCTCCGGCAACGCGTGTG	211
		antisense	AGTCCCTGCGGTCCGGACT	
HCN3	AF247452	sense	TGCCCCTCTCCCCTGATTC	335
		antisense	TTCCAGAGCCTTTGCGCCTA	

(*continued*)

Table 1. Continued

Gene	GenBank Accession no		Primers (from 5′ to 3′)	Fragment size (bp)
HCN4	AF247453	sense	AACCTGGGGGCTGGACAGA	462
		antisense	CTGGGCAGCCTGTGGAGAG	
SK2	U69882	sense	GCATGTGCACAACTTCATGATGGA	461
		antisense	CGCTCAGCATTGTAGGTGACATG	
Caa1A	M64373	sense	GAGCGGCTGGATGACACAGAAC	420
		antisense	CTGGCGACTCACCCTGGATGTC	
Caa1B	M92905	sense	TTGGCTCCTTCTTCATGCTCAAC	
		antisense	GATAAGGAACCGGAACATCTTCTC	409
Caa1G	AF027984	sense	TGGGCTCCTTCTTCATGATCAAC [CaT up]	
		antisense	GGAACTCTGAGCGTCCCATTAC	407
Caa1I	AF086827	sense	[CaT up]	
		antisense	AGGTCCGAGGAGACCCCATC	556
Cab1	X61394	sense	CCCTAAACTGCTGTGGGTGGA	
		antisense	CCCAGCTCTGCTCCCCAAAG	359
Cab2	M88751	sense	ACTGACCACCTCCTGCCCTAC	
		antisense	GTCCTGCCTCACCTGCACTG	555
Cab4	L02315	sense	GCTATGGTATTTGTTTGCTGGAAG	
		antisense	GACTGCAGAAGGAACAACACCTC	351

[1]Cauli *et al.* 1997; [2]Toledo-Rodriguez *et al.* 2004.

over neighbouring columns (horizontal diameter, mean ± S.D., 1013 ± 503 μm), and in some cases projecting as far as 2375 μm. In addition to the arborization in layer I, MCs also formed a local axonal arborization around their somata. Infragranular MCs formed an additional cluster of axons in layer IV. Axonal collaterals typically branched with large angles (about 80 deg on average) to form the arborization (Table 2). Finally, most MCs also sent a few axonal collaterals down to deeper layers without forming clusters.

A small fraction of MCs (5%) were consistently noticed to display much finer axons than most of the MCs (Table 2, AMC). A quantitative analysis revealed; (i) longer axonal segments, (ii) smaller and denser boutons (BD, $P < 0.05$), (iii) narrower axon branching angles (MABA, PABA, $P < 0.05$), and (iv) more axonal collaterals projecting towards deeper layers. Interestingly, they also seemed to present differences in the gene expression (see below). Such MCs were found in layer II/III ($n = 6$) and lower layers ($n = 3$).

Laminar specificity

Comparison between MCs located in different layers revealed layer specificity in morphologies of the dendritic and axonal arbours.

Layer II/III MCs. These MCs usually had the most extensive dendritic arbours. Most MCs (91%) projected their dendrites (mainly with a primary prominent dendrite) down to deeper layers, and more than half projected their dendrites as far as infragranular layers (layers V and VI). Their axonal collaterals were distributed mainly in layer I. Most MCs (74%) formed a more dense axonal cluster in layer I while the remainder formed a more dense axonal cluster around their own somata (Fig. 3*A*1). The clusters in layer I appeared as a secondary peak ∼350–370 μm from the somata in the axon Sholl distance histogram (ASD, reflecting the overall axonal spread, Fig. 3*A*2). On average, more than half (56%) of the total boutons of a layer II/III MC were distributed in layer I (see Table 2). These data indicate that layer I is the major target for layer II/III MCs.

Layer IV MCs. The dendritic distribution of layer IV MCs tended to be localized more within layer IV (43% with dendrites confined to layer IV; Fig. 3*B*1). The remainder of the MCs projected a few dendritic branches into neighbouring layers, but rarely further. Their dendritic trees were smaller than those of layers II/III and V MCs, presenting significantly shorter average lengths of dendritic trees (ALDT, $P < 0.05$, Table 2), shorter vertically spreading dendritic arbours ($P < 0.05$, Table 2), and smaller dendritic spread distance (DSD, reflects the overall dendritic spread, $P < 0.05$, Table 2). Their axon distribution also tended to be mostly restricted to their layer. They typically formed a prominent local axonal cluster around their somata (89% of layer IV MCs), sending only a few collaterals up to layer I which formed a sparse arborization, with a few horizontally projecting axons. Only a single peak close to the soma is therefore present in the ASD histogram (Fig. 3*B*2). Only 18% of the total boutons of layer IV MCs are distributed in layer I, which was significantly lower than both layer II/III

($P < 0.01$) and layer V MCs ($P < 0.05$; Table 2). Layer IV MCs generally also tended to present lower axonal branch orders (ABO), and smaller total axonal lengths compared with layer II/III MCs (Table 2).

Layer V MCs. The dendritic trees of layer V MCs were similar to those of layer II/III MCs. Seventy-three per cent distributed their dendrites mainly in the infragranular layers. We found that in addition to targeting layer I, the MCs also targeted layer IV. Most of these MCs formed larger axonal clusters in layer IV and in layer I than around their somata (94% of layer V MCs, Fig. 3*C*1). On average, most boutons were located in layer IV, but 36% were located in layer I (Table 2), suggesting that layer I is also a major target for layer V MCs. A typical layer V MC therefore presented two secondary peaks in the ASD histogram, one up to 520 μm away from the soma representing the axonal clusters formed in layer IV and another at ~750–850 μm away representing the axonal clusters formed in layer I (ASD, Fig. 3*C*2). Consistent with their deep location, layer V MCs presented a greater number of axonal segments (SEG), larger total axonal

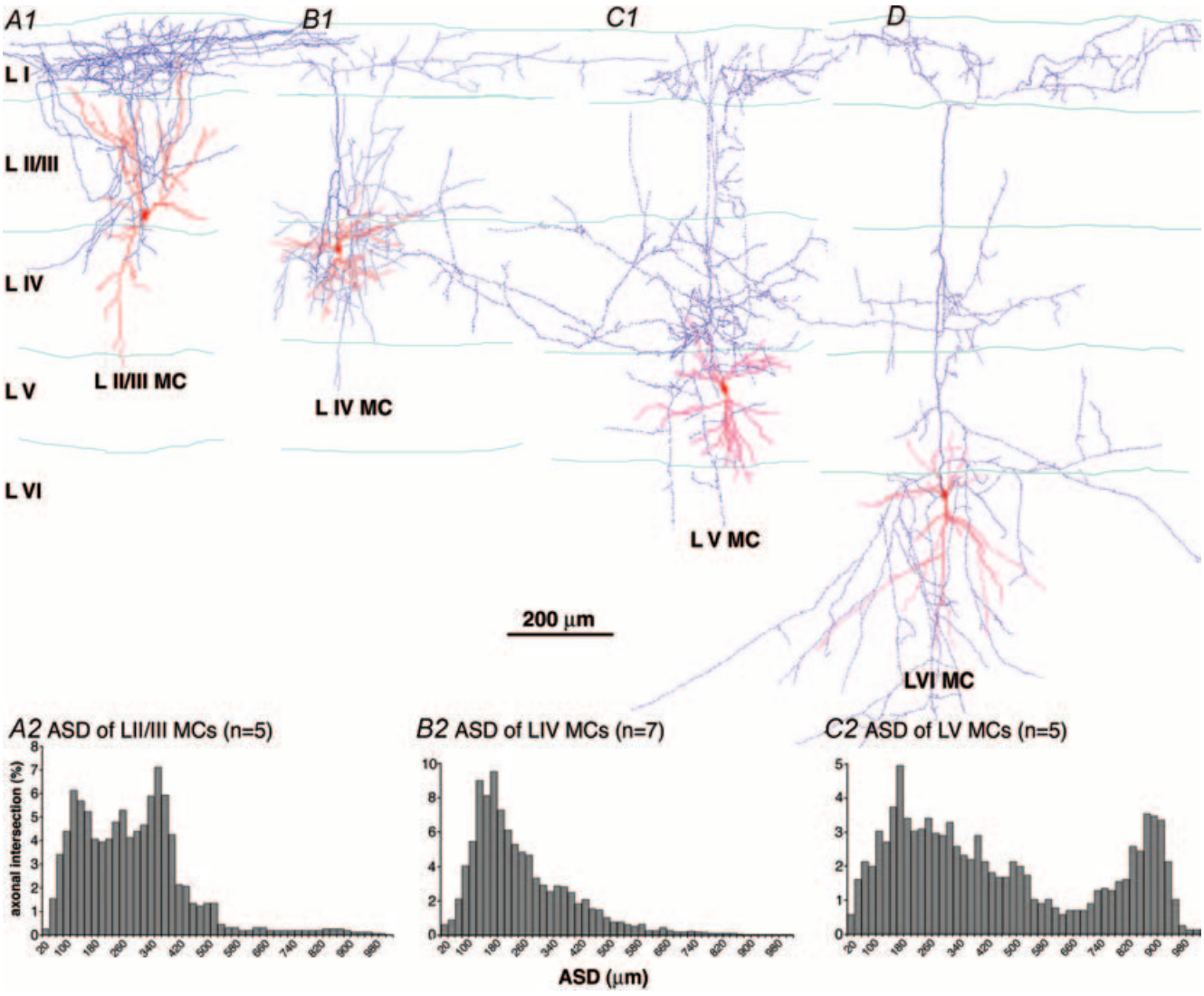

Figure 3. 3-D computer reconstructions of MCs in different layers
*A*1, layer II/III MC with a prominent axonal cluster in layer I and only a few collaterals ramified around its soma, and dendrites that extend vertically. *A*2, ASD distribution of layer II/III MCs displays two peaks. The first peak (around 100 μm) reflects the axonal cluster around soma. *B*1, layer IV MC with a prominent axonal cluster around the soma and sparse cluster in layer I, and localized dendrites. *B*2, ASD distribution of layer IV MCs. Only one peak was formed close to the soma. *C*1, layer V MC with a prominent axonal cluster in layers IV and I, a sparse cluster around the soma, and vertically extending dendrites. *D*, layer VI MC. This MC has a dendritic tree localized in the infragranular layers and an axonal tree forming clusters in layer I, IV and VI. *C*2, ASD distribution of layer V MCs also display two peaks.

Table 2. Comparison of anatomical properties of MCs

Anatomical properties	Reconstructed MCs				
	Total MC ($n = 24$)	MC in LII/III ($n = 5$)	MC in LIV ($n = 7$)	MC in LV ($n = 5$)	AMC in LII/III3 ($n = 5$)
Axonal					
Bouton/cell (BT) (mean ± S.D.)	3845 ± 1584	2880 ± 948	3146 ± 1258	3592 ± 1952	5302 ± 1527*
Bouton density (BD) (boutons/μm) (mean ± S.D.)	0.219 ± 0.047	0.197 ± 0.028	0.217 ± 0.038	0.173 ± 0.051	0.272 ± 0.037*
Maximum axonal branch angle (MABA, deg) (mean ± S.E.M.)	77 ± 1	83 ± 1	78 ± 1	81 ± 4	74 ± 1*
Planar axonal branch angle (MABA, deg) (mean ± S.E.M.)	54 ± 1	58 ± 1	55 ± 1	57 ± 4	50 ± 1*
Axon segment length (ASL, μm) (mean ± S.E.M.)	48 ± 3	43 ± 6	38 ± 2	53 ± 8	61 ± 9
ASD bouton no. (no. bouton/ASD unit) (mean ± S.E.M.)	275 ± 23	245 ± 25	222 ± 10	424 ± 85	249 ± 11
Axon Sholl distance (ASD) (μm) (mean ± S.E.M.)	285 ± 19	259 ± 24	236 ± 6	403 ± 78	292 ± 32
Maximum axonal branch order (ABO) (mean ± S.D.)	29.7 ± 10.1	30 ± 11	24 ± 5	44 ± 9	29 ± 8
Axonal segments/cell (SEG) (mean ± S.D.)	365 ± 139	340 ± 120	379 ± 133	426 ± 241	352 ± 95
Total axonal length (μm) (mean ± S.D.)	17813 ± 5535	14932 ± 5725	14061 ± 3368	19695 ± 6795	19272 ± 3419
Boutons in layer I per cell (%) (mean ± S.D.)	—	56 ± 20%	18 ± 7%†‡	36 ± 12%	—
Dendritic					
Average length of dendritic tree (ALDT, μm) (mean ± S.E.M.)	1504 ± 172	2103 ± 282	1093 ± 185†	1898 ± 548	1169 ± 368
Total dendritic length (μm) (mean ± S.D.)	3320 ± 1111	3252 ± 1027	2969 ± 736	4348 ± 1328	2630 ± 774
Diameter of dendritic cluster (horizontal, μm) (mean ± S.D.)	273 ± 88	212 ± 64	267 ± 88	364 ± 41*	200 ± 29
Diameter of dendritic cluster (vertical, μm) (mean ± S.D.)	490 ± 129	582 ± 122	362 ± 65†‡	499 ± 62	552 ± 65
Dendritic branch order (DBO) (mean ± S.E.M.)	6.5 ± 0.4	5.8 ± 0.7	6.1 ± 0.3	8.7 ± 1.4	5.4 ± 0.8
Maximum dendritic branch order (Max. DBO) (mean ± S.D.)	9.5 ± 2.5	8.8 ± 0.5	7.9 ± 1.7	10.5 ± 3.4	9.5 ± 2.5
Dendritic Sholl distance (DSD) (μm) (mean ± S.E.M.)	128 ± 6	142 ± 14	108 ± 4†‡	133 ± 13	129 ± 15
Dendritic segment length (DSL) (μm) (mean ± S.E.M.)	50 ± 2	55 ± 7	48 ± 3	51 ± 4	46 ± 4
Maximum dendritic branch angle (MDBA) (deg) (mean ± S.E.M.)	59 ± 2	61 ± 8	61 ± 3	64 ± 6	48 ± 4
Planar axonal branch angle (PDBA) (deg) (mean ± S.E.M.)	43 ± 2	44 ± 5	46 ± 2	47 ± 6	39 ± 3
Number of dendrites/cell (mean ± S.D.)	3.6 ± 1.3	3.8 ± 1.0	3.6 ± 1.1	2.5 ± 0.6	4.0 ± 1.4

†$P < 0.05$, significant comparison between MC in Layer II/III and MC in Layer IV; ‡$P < 0.05$, significant comparison between MC in Layer IV and MC in Layer V; *$P < 0.05$, significant comparison between MC and AMC (atypical MC) in Layer II/III.

lengths, overall axonal spread (ASD), higher branch orders (ABO) and more boutons and than MCs in layer II/III and IV (Table 2).

Layer VI MCs. These MCs were similar to those in layer V (Fig. 3*D*). Their dendrites mostly extended within infragranular layers (8/9). Like layer V MCs, they also formed axonal clusters in both layers IV and I, but more often formed denser axonal clusters around their somata (4/7) than found for layer V MCs (2/27).

In summary, these data reveal layer specificity of dendritic and especially axonal morphologies of MCs. Layer II/III MCs typically send their dendrites down to

deep layers and their axons up to target layer I. Layer IV MCs tend to restrict both dendrites and axons to layer IV. Layer V and VI MCs span the dendrites in the deeper layers, and send their axons up to layers IV and I.

Synaptic targets of Martinotti cells under EM

To examine the synaptic targets of MCs, random EM examination of MC boutons was obtained from seven MCs. From 130 boutons (including 7 boutons with two synaptic sites) 137 synapses were identified, which were all found to be symmetrical synapses (Fig. 4). Of these synapses, 71% were formed onto dendritic shafts (Fig. 4*A* and *B*) (42% onto PC shafts, 10% onto interneurone shafts and 19% onto dendritic shafts whose origins could not be identified), 22% onto spines (Fig. 4*C*), and 7% onto somata (Fig. 4*D*).

The synaptic target distribution was similar in the layer that the soma was located as compared with layer I. In the soma layer ($n = 102$), 71% of the boutons were formed onto dendritic shafts (43% onto PC shafts, 12% onto interneurone shafts and 16% onto dendritic shafts whose origins could not be identified), 22% onto spines, and 7% onto somata. In layer I ($n = 35$) 71% of the boutons were formed onto dendritic shafts (40% onto PC shafts, 6% onto interneurone shafts, 25% onto dendritic shafts whose origins could not be identified), 23% onto spines, and 6% onto somata. In layer I the ratio of synaptic targets onto interneurone shafts was smaller and the ratio of the unidentified shaft was larger compared with that in the soma region. This is probably because of the rich dendritic tufts in layer I originating mainly from PCs rather than interneurones.

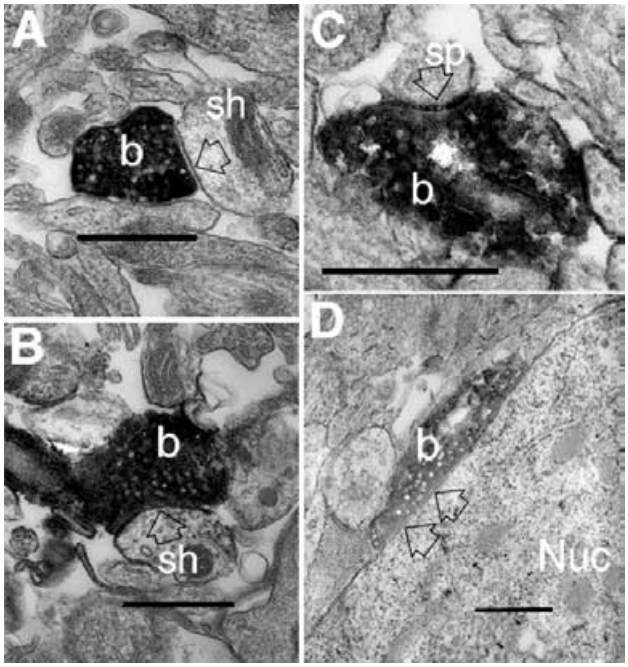

Figure 4. Random EM examination of MC boutons
A, MC boutons targeting a dendritic shaft of a putative PC. The synapse is pointed out with an unfilled wide arrow. Note the transmitter vesicles in the filled bouton and the postsynaptic shaft with light cytoplasm on the right. *B*, MC bouton targeting a dendritic shaft of a putative interneurone. Note the postsynaptic shaft with more cell organelles and darker cytoplasm. *C*, axo-spinous synapse. Note rigid and parallel pre-postsynaptic membrane appositions. *D*, axo-somatic synapse. Note synaptic vesicles along the presynaptic membrane and two active zones (rigid and parallel pre-postsynaptic membrane segments) indicated by two arrows. Nuc, nucleus; b, bouton; sh, dendritic shaft; sp, spine; arrow, synaptic junction; all scale bars, 0.5 μm.

Electrophysiology of Martinotti cells

Electrophysiological properties were obtained from the discharge responses to current injection in current-clamp mode. The electrophysiological properties were studied in detail for 127 out of the 180 MCs, which included 67 MCs recorded at 24–25°C (30 in layer II/III, 19 in layer IV, 14 in layer V and 4 in layer VI) and 60 MCs recorded at 34°C (13 in layer II/III, 10 in layer IV, 30 in layer V and 7 in layer VI).

Electrophysiological characteristics

MCs displayed diverse discharge responses to sustained somatic current injections. Responses were distinguished according to previously established criteria (see Methods; Gupta *et al.* 2000; Wang *et al.* 2002; Toledo-Rodriguez *et al.* 2003). The majority of the MCs displayed accommodating responses (AC, 90%) which is analogous to 'regular spiking' (Kawaguchi, 1995; Cauli *et al.* 1997), a small per cent displayed non-accommodating responses which is analogous to 'fast spiking' (NAC, 8%) and only a few MCs displayed irregular spiking responses (Kawaguchi & Kubota, 1993; Porter *et al.* 1999) (IS, 2%; see Table 3). The manner in which the neurones began their discharge (onset response) was also examined according to previously established criteria (see Methods) (Fig. 5). Of the ACs ($n = 115$), 84.5% displayed classical onset responses (c-AC) while 15.5% displayed burst onset responses (b-AC). All the NAC MCs ($n = 10$) displayed classical onset responses (c-NAC) while the two IS MCs started their response with a burst (b-IS) (Table 3). These responses were seen at 24–25 and 34°C, with the exception of the two IS responses, which were observed at 34°C.

Electrophysiological heterogeneity

In order to examine the electrophysiological properties of MCs in more detail, we applied a spectrum of stimulation protocols designed to capture key active and passive electrical properties (Fig. 6). The active properties studied

Table 3. Physiological classes and subclasses of MCs in different layers

Class	Subclass	Total	Layer II/III	Layer IV	Layer V	Layer VI
AC		115 (90%)	36 (83.7%)	26 (89.7%)	42 (95.5%)	11 (100%)
	b-AC	18 (14%)	5 (11.6%)	3 (10.4%)	9 (20.5%)	1 (9.1%)
	c-AC	97 (76%)	31 (72.1%)	23 (79.3%)	33 (75.0%)	10 (90.9%)
NAC	c-NAC	10 (8%)	7 (16.3%)	3 (10.3%)	—	—
STUT	b-STUT	2 (2%)	—	—	2 (4.5%)	—
All		127 (100%)	43 (34%)	29 (23%)	44 (35%)	11 (9%)

included characteristics of the AP and AHP waveform, and measurements of the discharge behaviour such as the rate of accommodation or irregular firing. The passive membrane properties studied included: *I–V* relationships, membrane time constants at different potentials, and membrane voltage decay following a brief hyperpolarizing current pulse. In order to standardize these profiles across all neurones, the amplitude of stimulation was normalized according to the minimal step current required to reach AP threshold. Subsequent analysis yielded 58 values that represent key active and passive properties of the neurone (Tables 4 and 6).

This analysis was separate and independent from the response classification of MCs mentioned above and was aimed at finding those electrical parameters that are the most uniform and those that are the most heterogeneous among MCs. The coefficient of variation of an electrical parameter across neurones was used as an index of heterogeneity. In general, parameters measuring similar electrical features had similar coefficients of variation (CV) (Table 5 and Fig. 7). The most uniform parameters (absolute CV < 0.1) across MCs were the threshold for AP generation and resting membrane potential. This is significant in view of the fact that interneurones, in general, can display wide variations in resting potentials (around 10 mV) and in action potential thresholds (around 20 mV). The action potential waveform was also highly uniform (first and second AP amplitude, total and half-width duration, rise and fall time).

MCs differ mostly in electrical parameters *after* the initial APs with the most varying electrical property being the AHP following a train of APs (the time constant and the amplitude of the AHP 100 ms after the burst). This was due to the fact that prominent AHPs were only present in a small fraction of MCs (corresponding to the c-NACs). The amplitude of the after-depolarization (ADP) was also highly variable, attributable to the presence of ADPs only in a subpopulation of MCs, especially in the b-ACs. The values describing the discharge response (extent of irregular spiking and accommodation) and the decrease in the amplitude of the AP during a spike train were also highly variable consistent with the many different response types found for MCs. These general patterns of the uniformity and heterogeneity of electrical properties seemed to apply to all layers.

Laminar specificity

The different response types of MCs were not evenly distributed throughout the cortical layers (Table 3). The accommodating MCs were found in all cortical layers, while NACs were found only in upper layers (layer II/III, 66% and IV, 34%) and bursting MCs were mostly found in layer V. Consistent with the different response types, layer IV MCs also presented with the lowest AP thresholds while layer VI presented with the highest (Table 4). Interestingly, opposite to the layer trend seen in PCs, upper layer MCs tended to display greater rectification in the *peak* and *steady-state* current–voltage curves (typically referred to as sag, due to I_h currents), than deeper layer MCs.

Molecular properties of Martinotti cells

To obtain the molecular expression profiles for the calcium binding proteins (CB, PV and CR) and the neuropeptides (NPY, VIP, SOM and CCK), single-cell RT-PCR was performed for 63 MCs located throughout layers II–VI (25 in layer II/III, 19 in layer IV, 14 in layer V, 5 in layer VI). Martinotti cells were found to be 100% SOM positive, PV negative and VIP negative ($n = 63$, Table 7). MCs are therefore distinct from basket cells, chandelier cells, some bipolar cells and bitufted cells in terms of their main patterns of expressing calcium binding proteins and neuropeptides (Fig. 8*C*).

Additionally, MCs with the highest quality of harvested mRNA (see Methods), were also screened for the expression of the voltage-activated K^+ channels (Kv1.1, Kv1.2, Kv1.4, Kv1.6, Kv2.1, Kv2.2, Kv3.1, Kv3.2, Kv3.3, Kv3.4, Kv4.2 and Kv4.3) and their auxiliary subunits (Kvβ1 and Kvβ2); the K^+/Na^+ permeable hyperpolarization-activated ion channels (HCN1, HCN2, HCN3 and HCN4); the Ca^{2+}-activated K^+ channel SK2 and the voltage-activated calcium channels (Caα1A, Caα1B, Caα1G and Caα1I) as well as their auxiliary subunits (Caβ1, Caβ3 and Caβ4) (see Table 1 for the list of primer pairs, the name and accession number of the genes amplified and the length of the PCR product).

Molecular heterogeneity

In more than half of the MCs, SOM was the only biochemical marker expressed (Table 7). The remaining

MCs co-expressed SOM with CB, CR, NPY or CCK. The majority of the co-expressions were with two biochemical markers and only three cases of co-expression with the three biochemical markers, SOM, CB and NPY, and 1 case with SOM, CB and CCK. There seemed to be some expression trends in MCs with different discharge responses. CCK was expressed only in the c-AC MCs ($n = 6/6$), while NPY was detected only in MCs with classical onset discharges ($n = 10$, 8 c-ACs, 2 c-NACs). NPY was also expressed in 2 of the 3 NACs examined. CB on the other hand, was expressed by MCs belonging to all three electrophysiological subtypes (c-AC, 9; b-AC, 2; c-NAC, 2). CB was also detected in all four of the rare slender axon MCs examined, while it was rarely expressed in the other MCs (15%, 6/35).

There was not sufficient data to make any statistically valid statements of layer specificity, but there seems to be a tendency for the lack of CCK expression in layer V MCs, lack of CB expression in layer VI MCs and presence of CR expression in layer IV (Table 7).

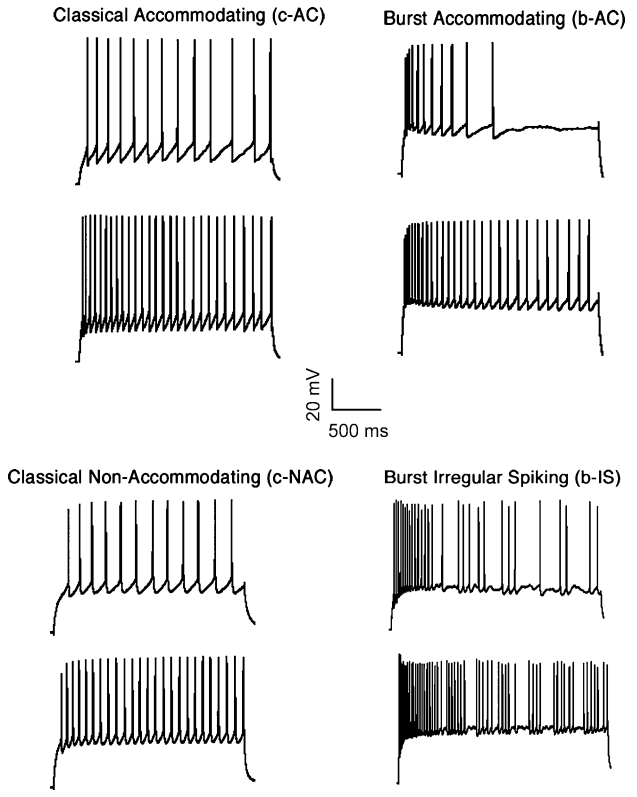

Figure 5. Four different discharge responses found in MCs
The discharge responses were induced by sustained somatic current injections. Top, accommodating (AC) responses show gradual increase in interspike intervals, including classical (c-AC, regular firing onset; top left) and bursting (b-AC, burst firing onset; top right). Bottom left, classical non-accommodating (c-NAC) cells display virtually no change in inter-spike intervals with regular firing onset. Bottom right, burst irregular spiking (b-IS) cells display abrupt changes in inter-spike intervals during steady state and bursting onset.

Ion channel expression

Frequency of expression is a poor index to describe the expression profile of neurones because of the uncertainties of harvesting and amplifying a particular mRNA, but positive expression is very informative and trends may be used as guidelines for future studies. MCs were screened for the expression of 26 K^+ and Ca^{2+} channel alpha and beta subunit genes including: (a) the voltage-activated K^+ channels (Kv1.1, Kv1.2, Kv1.4, Kv1.6, Kv2.1, Kv2.2, Kv3.1, Kv3.2, Kv3.3, Kv3.4, Kv4.2 and Kv4.3) and their auxiliary subunits (Kvβ1 and Kvβ2); (b) the K^+/Na^+-permeable hyperpolarization-activated ion channels (HCN1, HCN2, HCN3 and HCN4); (c) the Ca^{2+}-activated K^+ channel (SK2); (d) the voltage-activated calcium channels (Caα1A, Caα1B, Caα1G and Caα1I) and their auxiliary subunits (Caβ1, Caβ3 and Caβ4, Fig. 8*D*). We further examined only cells that expressed a minimum of 5 out of the 34 genes, including GAPDH, and only MCs that displayed c-AC responses, since this was the major response type ($n = 24$).

The ion channels with the highest detected expression (from highest to lowest) were Caβ1, Kv3.3, HCN4, Caβ4, Kv3.2, Kv3.1, Kv2.1, HCN3, Caα1G, Kv3.4, Kv4.2 and HCN2. SK2 expression was never detected in MCs (it has been detected in other types of interneurones using the same technique, Toledo-Rodriguez *et al.* 2004). It is interesting to note that Kv3.1 and Kv3.2 were also expressed in MCs, even though these ion channels have been related with fast spiking behaviour. The expression of these channels by themselves is therefore not sufficient to produce high frequency discharge or the co-expression of other genes in MCs prevents the development of fast firing behaviour.

MCs often display a depolarization following the AP (ADP) and we therefore examined the correlation between the presence of the ADP and the frequency of expression of some of the ion channel genes. From the 24 MCs whose ion channel expression was investigated, 8 presented ADPs (2.9 ± 2.7 mV; measured as mV after potential following the first AP generated in the AP threshold stimulus protocol) and the remainder showed no after potential at all. Of the four Na^+/K^+ ion channels tested, HCN2 was expressed more frequently in MCs with a prominent ADP (50% with ADP *versus* 25% without ADP). Conversely, HCN3 expression was more frequent in MCs without ADPs (25% with ADP *versus* 50% without ADP). From the high voltage Ca^{2+} channels, Caα1A was more expressed in MCs with ADPs (38% with ADP *versus* 19% without ADP). In contrast, some of the low voltage Ca^{2+} channels showed no or a mild expression preference (Caα1I 13% with ADP *versus* 6% without ADP; Caα1G 38% in both cases). Finally, A-type K^+ channels such as Kv4.2 were more frequently detected in MCs without ADPs (13%

with ADP *versus* 38% without ADP). Kv2.1 was also more frequently detected in MCs without ADPs (13% with ADP *versus* 56% without ADP). While this study shows which genes can be expressed in MCs, the number of MCs in this analysis ($n = 24$) is too low for rigorous statistical validation of comparisons and the descriptions should be viewed only as guidelines for future studies.

Discussion

Summary

The present study provides the first detailed anatomical, electrophysiological and molecular analysis of Martinotti cells in layers II to VI of rat somatosensory cortex. The study yielded features common to MCs in all layers, layer-specific morphological and electrophysiological properties, as well as the multidomain, multilayer and cross-columnar targeting nature of MCs. MCs are mostly bitufted and accommodating interneurones always express SOM but never express PV or VIP and target layer I. Morphologically, the main dendritic axis is down towards deeper layers while the axonal focus is up toward layer I. MCs are specialized to target multiple layers including the same layer where the soma is located, layer IV and layer I. Electrophysiologically, MCs are shown to display different discharge responses in different layers with a tendency for accommodating MCs to be located in all layers, non-accommodating MCs to be located in upper layers and bursting MCs in deeper layers. Molecularly, the study confirms previous works showing that SOM is commonly expressed in MCs and extends these findings not only by demonstrating that SOM expression as an essential property of all MCs in all layers, but also that the lack of PV and VIP is an essential part of their molecular profile. We further find that MCs can express CR, NPY and CCK, which may depend on the layer in which the MC is located. Finally, we show for the first time, using the single-cell multiplex RT-PCR approach, the expression of ion channel genes in MCs (from highest to lowest); Caβ1, Kv3.3, HCN4, Caβ4, Kv3.2, Kv3.1, Kv2.1, HCN3, Caα1G, Kv3.4, Kv4.2, Kv1.1 and HCN2; are most often detected

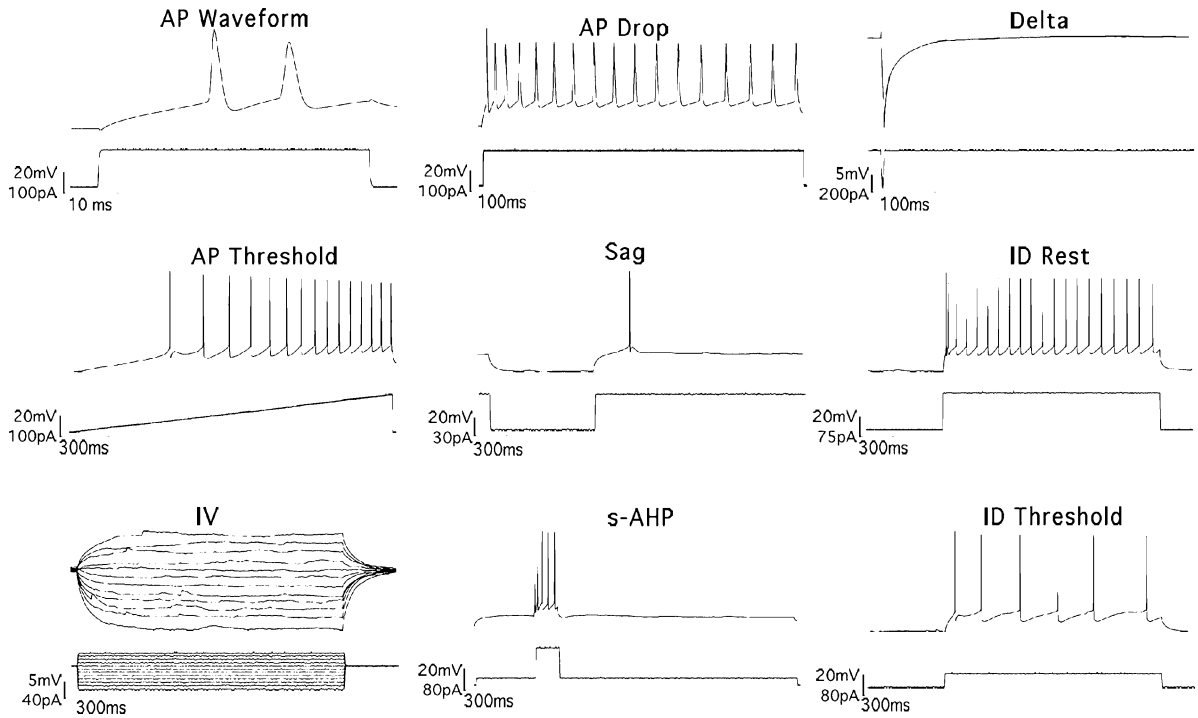

Figure 6. Major electrophysiological parameters for active and passive properties of MCs
Example responses to different stimulation protocols used for electrophysiological characterization. AP Waveform, APs evoked by brief step current injections. AP Threshold, the threshold for AP discharge was measured during a ramp current injection. AP Drop, changes in AP amplitude during a discharge train evoked by a step current injection. IV, the current–voltage relationship was extracted by a series of subthreshold current injections. Delta, the response to a brief (1 ms) hyperpolarizing current was used to measure the membrane time constant. Sag, the response to a hyperpolarizing current step was analysed to reveal the existence of hyperpolarization-dependent inward currents. s-AHP, the existence and degree of slow membrane hyperpolarization following rapid discharge. ID Rest, discharge response to increasing current injections was used for assessing the current-discharge properties of MCs. ID Threshold, discharge response to near-threshold current injections, used for neuronal classification by revealing the existence of onset delays or bursts.

Table 4. Comparison of electrophysiological properties of MCs in different layers at RT

	Mean ± S.D.					*t* test					
	All layers ($n = 67$)	Layer II/III ($n = 30$)	Layer IV ($n = 19$)	Layer V ($n = 14$)	Layer VI ($n = 4$)	LII/III *vs* LIV	LII/III *vs* LV	LII/III *vs* LVI	LIV *vs* LV	LIV *vs* LVI	LV *vs* LVI
Resting mV	−54.57±5.06	−54.85±4.77	−54.59±6.57	−54.57±4.24	−52.50±4.20						
AP drop											
Drop in 1st to 2nd spike (mV)	3.95±4.98	2.43±4.17	6.62±4.84	3.69±5.52	3.59±6.60	$P < 0.01$					
Change to SS (mV)	7.12±9.16	6.04±9.37	11.77±8.34	4.03±7.30	3.95±13.00	$P < 0.05$			$P < 0.01$		
Change to SS after 2nd spike (mV)	−3.17±5.87	−3.61±6.74	−5.16±4.67	−0.33±4.24	−0.35±6.89				$P < 0.01$		
Max rate of AP change (mV/AP)	1.19±1.05	1.22±1.28	0.73±0.50	1.60±1.00	1.70±0.66				$P < 0.01$		
AP1 waveform											
AP ampl., av (mV)	68.52±8.94	65.99±7.96	75.00±9.60	66.26±7.12	64.60±5.19	$P < 0.01$			$P < 0.01$	$P < 0.05$	
AP duration, av (ms)	3.49±0.45	3.40±0.46	3.69±0.53	3.42±0.31	3.46±0.10						
AP duration HW, av (ms)	1.62±0.25	1.57±0.23	1.71±0.31	1.64±0.23	1.62±0.03						
AP rise time, av (ms)	1.11±0.19	1.10±0.22	1.13±0.21	1.11±0.14	1.10±0.05						
AP fall time, av (ms)	2.37±0.30	2.29±0.26	2.55±0.38	2.31±0.20	2.36±0.05	$P < 0.05$			$P < 0.05$	$P < 0.05$	
AP rise rate (mV ms^{-1})	63.83±13.81	61.94±13.23	70.53±16.92	61.29±11.26	58.50±2.92					$P < 0.05$	
AP fall rate (mV ms^{-1})	−29.38±10.25	−29.46±10.15	−28.39±14.78	−30.21±4.90	−30.15±1.31						$P > 0.95$
AHP fast, av (mV)	8.67±3.79	9.30±2.98	6.70±4.38	8.95±4.03	12.31±1.72	$P < 0.05$		$P < 0.05$		$P < 0.01$	$P < 0.05$
AP2 waveform											
AP ampl., av (mV)	62.29±7.36	60.51±6.79	67.31±8.40	60.80±5.91	59.49±2.54	$P < 0.01$			$P < 0.05$	$P < 0.01$	
AP duration, av (ms)	4.17±0.50	4.16±0.55	4.32±0.53	4.03±0.42	4.11±0.24						
AP duration HW, av (ms)	2.07±0.33	2.07±0.39	2.12±0.31	2.00±0.27	2.06±0.16						
AP rise time, av (ms)	1.37±0.23	1.39±0.26	1.36±0.21	1.36±0.22	1.36±0.15						
AP fall time, av (ms)	2.80±0.35	2.78±0.35	2.97±0.43	2.67±0.25	2.75±0.10				$P < 0.05$		
AP rise rate (mV ms^{-1})	46.84±10.37	45.21±9.94	51.01±12.43	46.34±9.62	44.13±5.82						
AP fall rate (mV ms^{-1})	−22.41±5.85	−21.19±7.68	−23.19±3.80	−23.81±3.65	−23.60±1.58						
AHP fast, av (mV)	9.72±2.33	9.50±2.48	9.05±1.60	10.16±2.60	12.59±0.75			$P < 0.01$		$P < 0.01$	$P < 0.01$
AP1/AP2 waveform											
Ch, AP ampl. (%)	−10.01±6.30	−9.12±5.46	−12.67±6.81	−9.07±6.32	−8.73±9.85						
Ch, AP duration (%)	16.95±4.83	17.98±5.89	16.97±3.69	15.08±3.59	15.63±2.94						
Ch, AP duration HW (%)	22.64±7.18	25.02±8.47	22.30±5.26	18.35±4.98	21.19±4.71		$P < 0.01$		$P < 0.05$		

Ch, AP rise rate (%)	−38.24±16.48	−38.24±14.70	−43.00±18.65	−33.82±17.00	−34.62±21.91						
Ch, AP fall rate (%)	−34.80±12.84	−38.06±14.16	−37.17±11.37	−26.98±8.49	−28.29±11.93		$P < 0.01$		$P < 0.01$		
Ch, AHP fast (%)	9.43±25.41	2.04±19.84	15.51±17.65	19.38±40.28	2.30±11.69	$P < 0.05$					
ADP											
The ADP (mV)	1.07±2.10	0.39±1.58	0.96±1.96	2.79±2.63	1.13±2.25		$P < 0.01$		$P < 0.05$		
IV											
IR for peak (MΩ)	330.19±134.87	287.63±99.18	376.03±162.92	371.98±156.52	285.43±59.05	$P < 0.05$					
IR for SS (MΩ)	198.19±79.87	173.25±64.25	230.61±95.21	212.41±87.54	181.51±27.48	$P < 0.05$					
RI for peak IV	28.22±10.94	30.57±12.03	30.59±11.91	21.40±4.25	23.29±1.99		$P < 0.01$	$P < 0.01$	$P < 0.01$	$P < 0.05$	
RI for SS IV	17.47±8.24	19.00±9.55	19.16±8.31	12.57±3.44	15.05±2.45		$P < 0.01$		$P < 0.01$		
Max sag is (mV)	4.63±2.71	5.44±2.72	3.46±1.92	3.84±2.78	6.91±3.44	$P < 0.01$					
Delta											
Delta av decay time constant (ms)	24.00±8.37	22.77±6.78	25.57±8.34	25.59±12.06	20.13±2.96					$P < 0.05$	
AP threshhold											
AP threshold (mV)	−47.10±2.99	−46.27±2.92	−48.96±1.33	−47.09±3.95	−44.44±1.06	$P < 0.01$		$P < 0.05$		$P < 0.01$	$P < 0.05$
AHP after 1st AP in the ramp	9.09±3.49	9.21±3.31	8.05±2.40	8.61±4.02	14.71±3.30			$P < 0.05$		$P < 0.05$	$P < 0.05$
sAHP											
sAHP, 0.8 ms (mV)	0.79±2.23	1.12±1.67	0.56±2.76	0.21±2.78	1.53±1.02						
sAHP, max (mV)	2.00±1.68	2.09±1.43	1.46±1.93	2.12±1.73	3.29±2.06						
Time, max (ms)	0.99±0.41	0.95±0.39	0.98±0.48	1.06±0.44	1.03±0.34						
sAHP, τ (ms)	238.54±764.27	142.26±242.72	40.90±96.39	441.68±851.02	1140.23±2705.74						
Sag											
Max sag	10.90±4.83	12.75±4.50	8.18±2.77	10.57±6.20	8.31±2.36	$P < 0.01$		$P < 0.05$			
Sag Vs. VmSlope	−0.16±0.07	−0.19±0.07	−0.14±0.04	−0.13±0.07	−0.13±0.03	$P < 0.05$	$P < 0.01$	$P < 0.05$			
Rebound spike	0.60±0.49	0.50±0.51	0.73±0.47	0.69±0.48	0.50±0.58						
Discharge											
Slope of ID threshold	0.18±0.06	0.19±0.05	0.20±0.07	0.15±0.08	0.12±0.02			$P < 0.01$		$P < 0.01$	
Av delay to 1st spike	0.05±0.03	0.05±0.02	0.06±0.03	0.05±0.03	0.04±0.02						
SD for delay to 1st spike	0.06±0.04	0.05±0.04	0.07±0.05	0.05±0.03	0.05±0.04						
Av delay to 2nd spike	0.06±0.03	0.07±0.03	0.08±0.04	0.05±0.02	0.05±0.02		$P < 0.05$		$P < 0.05$		
SD for delay to 2nd spike	0.07±0.07	0.08±0.08	0.09±0.08	0.05±0.03	0.04±0.02		$P < 0.05$	$P < 0.05$		$P < 0.05$	
Av initial burst interval	0.06±0.04	0.06±0.03	0.08±0.04	0.05±0.02	0.05±0.02		$P < 0.05$		$P < 0.05$	$P < 0.05$	
SD for av initial burst interval	0.07±0.07	0.08±0.08	0.09±0.08	0.05±0.03	0.04±0.02		$P < 0.05$	$P < 0.05$	$P < 0.05$	$P < 0.05$	
Av initial accom	−38.87±49.81	−24.73±30.61	−39.35±39.18	−73.05±81.73	−23.02±20.32		$P < 0.05$				
Av SS accom	−148.84±167.90	−87.70±63.77	−112.48±83.77	−291.23±284.98	−281.76±179.89		$P < 0.05$		$P < 0.05$		
Rate of accom I toSS	−14.09±21.28	−6.78±7.16	−10.00±9.10	−31.97±38.44	−25.78±19.95		$P < 0.05$				
Av accom at SS	−16.30±35.24	−7.56±5.93	−13.41±11.60	−28.91±69.30	−51.45±50.67						
Av rate accom during SS	−1.95±5.02	−0.75±0.72	−1.52±1.50	−3.90±9.94	−6.07±7.69	$P < 0.05$					
Av CV discharge	6.25±3.75	7.90±4.04	5.97±3.29	3.91±2.22	3.42±2.33		$P < 0.01$	$P < 0.05$	$P < 0.05$		
Av skew discharge	−0.35±0.90	−0.47±0.82	−0.32±0.81	−0.38±0.92	0.53±1.73						
Av discharge STUT	0.09±0.08	0.06±0.04	0.09±0.07	0.14±0.09	0.18±0.12	$P < 0.01$					

SS, steady state; RI, rectification index; IR, input resistance; AP, action potential; HW, half-width; sAHP; small after hyperpolarization; SD, standard deviation.

Table 5. Variance of the electrophysiological properties of MCs

No.	Physiological properties	CV all layers ($n = 67$)	CV layer II/III ($n = 30$)	CV layer IV ($n = 19$)	CV layer V ($n = 14$)	CV layer VI ($n = 4$)
35	AP threshhold – AP threshold (mV)	0.06	0.06	0.03	0.08	0.02
1	mV – Resting mV	0.09	0.09	0.12	0.08	0.08
14	AP2 waveform – AP ampl., av (mV)	0.12	0.11	0.12	0.10	0.04
15	AP2 waveform – AP duration, av (ms)	0.12	0.13	0.12	0.10	0.06
18	AP2 waveform – AP fall time, av (ms)	0.13	0.13	0.15	0.09	0.04
10	AP1 waveform – AP fall time, av (ms)	0.13	0.11	0.15	0.09	0.02
7	AP1 waveform – AP duration, av (ms)	0.13	0.14	0.14	0.09	0.03
6	AP1 waveform – AP ampl., av (mV)	0.13	0.12	0.13	0.11	0.08
8	AP1 waveform – AP durationHW, av (ms)	0.15	0.15	0.18	0.14	0.02
16	AP2 waveform – AP duration HW, av (ms)	0.16	0.19	0.15	0.13	0.08
17	AP2 waveform – AP rise time, av (ms)	0.17	0.19	0.16	0.16	0.11
9	AP1 waveform – AP rise time, av (ms)	0.17	0.20	0.19	0.12	0.04
11	AP1 waveform – AP rise rate (mV ms^{-1})	0.22	0.21	0.24	0.18	0.05
19	AP2 waveform – AP rise rate (mV ms^{-1})	0.22	0.22	0.24	0.21	0.13
21	AP2 waveform – AHP fast, av (mV)	0.24	0.26	0.18	0.26	0.06
20	AP2 waveform – AP fall rate (mV ms^{-1})	0.26	0.36	0.16	0.15	0.07
23	AP1/AP2 waveform – Ch AP duration (%)	0.28	0.33	0.22	0.24	0.19
24	AP1/AP2 waveform – Ch AP duration HW (%)	0.32	0.34	0.24	0.27	0.22
34	Delta – Delta av decay time constant (ms)	0.35	0.30	0.33	0.47	0.15
12	AP1 waveform – AP fall rate (mV ms^{-1})	0.35	0.34	0.52	0.16	0.04
44	Discharge – slope of ID threshold	0.35	0.29	0.33	0.49	0.15
26	AP1/AP2 waveform – Ch AP fall rate (%)	0.37	0.37	0.31	0.31	0.42
36	AP threshhold – AHP after 1st AP in ramp	0.38	0.36	0.30	0.47	0.22
31	IV – rectification index for peak IV	0.39	0.39	0.39	0.20	0.09
30	IV – input resistance for SS (MΩ)	0.40	0.37	0.41	0.41	0.15
29	IV – input resistance for peak (MΩ)	0.41	0.34	0.43	0.42	0.21
42	Sag – Sag Vs Vm slope	0.42	0.36	0.31	0.53	0.25
39	sAHP – time max (ms)	0.42	0.41	0.49	0.42	0.33
25	AP1/AP2 waveform – Ch_AP rise rate (%)	0.43	0.38	0.43	0.50	0.63
13	AP1 waveform – AHPfast_av (mV)	0.44	0.32	0.65	0.45	0.14
41	Sag – max Sag	0.44	0.35	0.34	0.59	0.28
32	IV – rectification index for SS IV	0.47	0.50	0.43	0.27	0.16
45	Discharge – av delay to 1st spike	0.51	0.48	0.51	0.61	0.37
47	Discharge – av delay to 2nd spike	0.54	0.47	0.59	0.46	0.36
49	Discharge – av initial burst interval	0.55	0.49	0.58	0.51	0.36
33	IV – max Sag is (mV)	0.59	0.50	0.55	0.72	0.50
56	Discharge – av CV discharge	0.60	0.51	0.55	0.57	0.68
22	AP1/AP2 waveform – Ch AP ampl. (%)	0.63	0.60	0.54	0.70	1.13
46	Discharge – SD for delay to 1st spike	0.70	0.71	0.73	0.63	0.69
58	Discharge – Av discharge STUT	0.80	0.68	0.75	0.66	0.65
43	Sag – rebound spike	0.82	1.02	0.64	0.69	1.15
38	sAHP – sAHP, max (mV)	0.84	0.68	1.32	0.82	0.63
5	AP drop – max rate of AP change (mV/AP)	0.88	1.05	0.68	0.63	0.39
50	Discharge – SD for av initial burst interval	0.94	0.93	0.91	0.71	0.50
48	Discharge – SD for delay to 2nd spike	0.96	0.94	0.94	0.71	0.50
52	Discharge – av SS accom	1.13	0.73	0.74	0.98	0.64
2	AP drop – drop in 1st to 2nd spike (mV)	1.26	1.72	0.73	1.49	1.84
51	Discharge – av initial accom	1.28	1.24	1.00	1.12	0.88
3	AP drop – change to SS (mV)	1.29	1.55	0.71	1.81	3.29
53	Discharge – rate of accom I to SS	1.51	1.06	0.91	1.20	0.77
4	AP drop – change to SS after 2nd spike (mV)	1.85	1.87	0.91	12.73	19.51
28	ADP – The ADP (mV)	1.96	4.08	2.04	0.94	2.00
54	Discharge – av accom at SS	2.16	0.78	0.86	2.40	0.98
55	Discharge – av rate accom during SS	2.58	0.96	0.99	2.55	1.27
57	Discharge – av skew discharge	2.61	1.76	2.54	2.40	3.25
27	AP1/AP2 waveform – Ch AHP fast (%)	2.69	9.71	1.14	2.08	5.09
37	sAHP – sAHP, 0.8 ms (mV)	2.81	1.49	4.96	13.14	0.67
40	sAHP – sAHP, τ(ms)	3.20	1.71	2.36	1.93	2.37

in c-AC MCs. Additionally, HCN2 and the high threshold calcium channels seem to be more expressed in c-AC MCs that display ADPs. The data also shows that MCs express Kv3.1, which is a powerful delayed rectifier commonly expressed in fast spiking interneurones. Low voltage-activated calcium channels, as well as ion channel genes supporting A-type currents, can be expressed by MCs. In conclusion, this study provides deeper insight into the morphological, electrophysiological and molecular design of MCs and reveals the anatomical substrate for a crucial role in multiple inhibitory feedback loops within and between cortical columns.

Morphology

Martinotti cells constitute roughly 16.5% of the interneurones in somatosensory cortex of young rats (authors' unpublished estimates). The proximal dendritic arbour is bipolar or bitufted in nearly 90% of cases with an ovoid or spindle-like soma and can only be approximately identified using IR-DIC microscopy. MCs can, however, be identified easily after staining, by two unique axonal features – the axonal arborization in layer I and spiny boutons. The axonal arborization in layer I can extend to most of the neighbouring and even to more distal columns as far as 2 mm away. MCs are also unique in terms of their dendritic morphology – they display the most elaborate dendritic arbours of all interneurones (authors' unpublished data) and they bear spines more often on their dendrites at this stage of development. Since interneurones are essentially spine free after maturation (Fairen *et al.* 1984), this perhaps suggests that MCs complete their maturation slower than other interneurones.

Electrophysiology and ion channel expression

Previous reports indicated that MCs can respond with 'regular' and 'burst' firing in response to depolarizing somatic current injections and that the threshold for discharging responses is low (referred to as low threshold spiking, LTS) (Kawaguchi, 1995; Kawaguchi & Kubota, 1997; see also Goldberg *et al.* 2004). In this study, we found three main response types with 90% accommodating (regular spiking), 8% non-accommodating and 2% irregular spiking responses. The bursting response type was found in a subset of the accommodating and all of the irregular spiking MCs, making up a total of about 17% of all MCs. These data are therefore consistent with findings in the adult rat and further show that some MCs can display fast spiking responses and provide estimates of the frequencies of occurrences of the different response types.

The spike train accommodation found in most MCs superficially appears similar to regular spiking in PCs, but the responses are different in many respects. The most important difference is that, while accommodation in PCs is caused by AHPs due to Ca^{2+}-activated K^+ outward conductances, MCs lack AHPs, as well as the SK2 ion channel that produces Ca^{2+}-activated K^+ currents; instead MCs display ADPs more often. Further studies are required to determine which ion channels contribute towards MC accommodation.

Many MCs, especially deep layer MCs, display bursting behaviour. Prominent after-depolarizations, which facilitate bursting, are commonly found in accommodating MCs and not in non-accommodating MCs. The ADP is believed to result from the combined activity of the hyperpolarization-activated Na^+/K^+ channels (HCN1–HCN4). Indeed, the hyperpolarization-activated Na^+/K^+ channel (HCN2) seems to be more expressed in MCs presenting ADPs,

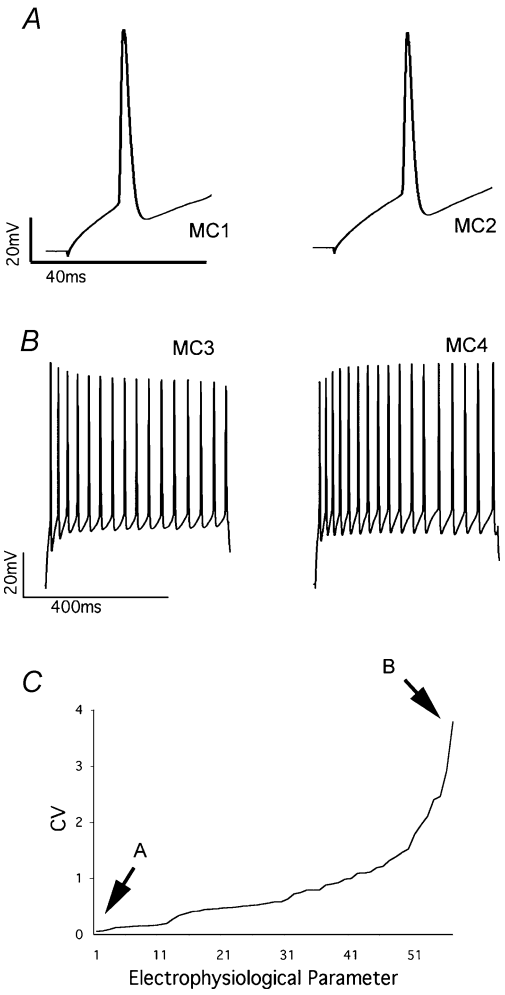

Figure 7. Representative samples of electrophysiological parameters with the highest and lowest coefficient of variation
A, AP waveform traces. Some of the AP parameters showed the lowest coefficient of variation. *B*, AP drop traces. Some of the AP drop parameters showed the highest coefficient of variation. *C*, graph describing the absolute CVs for different electrophysiological parameters sorted from the less to the most variable. See Table 5 for the identity of the electrophysiological parameters.

Table 6. Comparison of electrophysiological properties of MCs at 34°C

	Layer V ($n = 25$)	Layer VI ($n = 7$)
AP1 waveform		
AP ampl., av (mV)	54.97 ± 12.29	52.57 ± 9.22
AP duration, av (ms)	3.45 ± 0.83†	2.97 ± 0.24
AP duration HW, av (ms)	1.57 ± 0.33	1.44 ± 0.36
AP rise time, av (ms)	1.19 ± 0.22	1.11 ± 0.16
AP fall time, av (ms)	2.26 ± 0.62†	1.86 ± 0.09
AP rise rate (mV ms^{-1})	47.20 ± 11.11	48.69 ± 12.16
AP fall rate (mV ms^{-1})	−27.74 ± 7.13	−33.19 ± 10.31
AHP fast, av (mV)	7.34 ± 11.92	13.40 ± 7.28
AP2 waveform		
AP ampl., av (mV)	52.06 ± 8.97	55.55 ± 11.13
AP duration, av (ms)	3.72 ± 0.79	3.36 ± 0.19
AP duration HW, av (ms)	1.75 ± 0.36	1.66 ± 0.32
AP rise time, av (ms)	1.32 ± 0.26	1.25 ± 0.19
AP fall time, av (ms)	2.41 ± 0.57†	2.11 ± 0.09
AP rise rate (mV ms^{-1})	40.77 ± 9.35	45.98 ± 13.14
AP fall rate (mV ms^{-1})	−24.45 ± 5.77	−29.91 ± 8.35
AHP fast_av (mV)	10.84 ± 3.44	13.24 ± 5.05
AP1/AP2 waveform		
Ch AP ampl. (%)	−3.14 ± 10.69	4.80 ± 4.44
Ch AP duration (%)	10.01 ± 4.11	11.66 ± 2.94
Ch AP duration HW (%)	12.42 ± 5.18	13.63 ± 4.23
Ch AP rise rate (%)	−17.16 ± 19.69	−7.18 ± 5.64
Ch AP fall rate (%)	−14.84 ± 16.80	−9.89 ± 6.05
Ch AHP fast (%)	15.13 ± 59.00	10.22 ± 40.89
IV		
Input resistance for peak (MΩ)	326.21 ± 196.53	228.68 ± 119.89
Input resistance for SS (MΩ)	254.44 ± 166.89	171.50 ± 81.20
Rectification index for peak IV	21.79 ± 10.71	18.47 ± 2.27
Rectification index for SS IV	16.70 ± 6.26	14.31 ± 2.97
Maximum Sag is (mV)	4.44 ± 4.17	5.37 ± 2.78
Delta		
Delta av decay time constant (ms)	17.57 ± 9.24	34.05 ± 27.38
AP threshhold		
AP threshold (mV)	−46.09 ± 5.54	−43.25 ± 1.15
AHP after 1st AP in the ramp	7.49 ± 3.40	11.83 ± 5.83
sAHP		
sAHP max (mV)	2.61 ± 2.61	6.55 ± 7.15
sAHP τ (ms)	1693.90 ± 1227.04	–
Discharge		
Slope of ID threshold	0.15 ± 0.06	0.12 ± 0.10
Av delay to 1st spike	0.06 ± 0.03	0.05 ± 0.03
SD for delay to 1st spike	0.05 ± 0.05	0.05 ± 0.03
Av delay to 2nd spike	0.06 ± 0.03	0.05 ± 0.01
SD for delay to 2nd spike	0.04 ± 0.02	0.06 ± 0.04
Av initial burst interval	0.05 ± 0.03	0.05 ± 0.02
SD for av initial burst interval	0.04 ± 0.03	−25.43 ± 56.99
Av initial accom	−44.74 ± 35.67	−95.61 ± 102.10
Av SS accom	−212.19 ± 172.70	−89.00 ± 68.49
Rate of accom ItoSt	−19.10 ± 16.58	−23.74 ± 34.75
Av accom at SS	−30.54 ± 58.30	−5.62 ± 9.95
Av rate accom during SS	−3.43 ± 7.22	−0.09 ± 1.84
Av CV discharge	3.32 ± 1.76	2.93 ± 2.15
Av skew discharge	0.13 ± 1.45	−0.45 ± 0.67
Av discharge STUT	0.15 ± 0.12	12.30 ± 27.33

†$P < 0.05$, comparison between different layers.

Table 7. Co-expression patterns of calcium binding proteins and neuropeptides mRNA of different layer MCs

	n	SOM + CB	Only SOM + PV	SOM + CR	SOM + NPY	SOM + VIP	SOM + CCK	SOM + CB	SOM + NPY	SOM + CB	SOM + CCK
All Layers	63	100.0%	55.6%	15.9%	—	3.2%	12.7%	—	7.9%	3.2%	1.6%
Layer II/III	25	100.0%	60.0%	12.0%	—	—	12.0%	—	8.0%	4.0%	4.0%
Layer IV	19	100.0%	52.6%	26.3%	—	10.5%	—	—	5.3%	5.3%	—
Layer V	14	100.0%	64.3%	14.3%	—	—	21.4%	—	—	—	—
Layer VI	5	100.0%	20.0%	—	—	—	40.0%	—	40.0%	—	—

but the ADP is not the only cause of bursting in MCs since some non-bursting MCs can also display ADPs. The MCs, however, seem to lack the T-type voltage-activated Ca^{2+} channel Caα1I which may be required to boost the depolarization to trigger a burst.

Layer-specific electrophysiology

This study revealed that MCs can respond differently to depolarizing input. Some of these differences seem to depend on the layer in which the interneurone is located. We found that the AP threshold is lowest for layer IV MCs and highest for layer VI MCs. This may pre-dispose to earlier activation of layer IV MCs at the onset of processing in the microcircuit and later stage activation of layer VI MCs at a more advanced stage of microcircuit processing. Indeed, several *in vivo* studies have shown that putative inhibitory neurones in layer IV respond most vigorously at low thresholds and with short latencies (Simons, 1978; Yamamoto *et al.* 1988; Swadlow, 1989). Layer VI MCs were actually found to display the highest thresholds of all interneurones (data not shown) suggesting that they permit the most elaborate integration. This may be important to allow specific thalamic input to escalate to a critical level via the positive feedback loop between layer VI PCs and thalamic neurones, before layer VI MCs would break the positive feedback loop.

The various electrophysiological subtypes, while much less frequent, may also be important to allow MCs to perform multiple tasks. For example, most bursting MCs were located in layer V where many intrinsic bursting PCs are also commonly found. These bursting PCs are the main neurones providing the output to subcortical regions (see De la Pena & Geijo-Barrientos, 1996). Bursting could make signal transmission more intense and reliable and the higher fraction of bursting MCs in layer V may therefore be important for resetting the cortical column after moments of intense output.

Biochemical properties

Previous immunohistochemical studies have reported that MCs belong to the group of SOM-positive interneurones (Wahle, 1993; Kawaguchi & Kubota, 1997; Kawaguchi & Kubota, 1998). We confirm this finding at the mRNA level and further show that SOM is expressed by *all* MCs and in *all* layers regardless of their anatomical and electrophysiological differences. SOM is a neuropeptide that acts as a co-released inhibitory neurotransmitter by opening different types of potassium channels (Tallent & Siggins, 1997). SOM also activates the delay rectifier channels in cultured neocortical neurones. In the solitary nucleus SOM inhibition occurs through hyperpolarization and augmentation of a non-inactivating voltage-dependent outward current blocked by muscarinic agonists (I_M). SOM also augments the I_M current in CA1 hippocampal neurones, inhibits calcium currents in rat neocortical neurones, and reduces N-type currents in dissociated hippocampal PCs. The potential regulatory activity of SOM is even more complex when one takes into account that the SOM gene gives rise to two main biologically active products, SOM 14 and SOM 28. Both of these are believed to act as neurotransmitters showing opposite effects on K^+ currents in rat neocortical neurones. A single MC can therefore exert a complex modulatory effect on the microcircuit (for references see Schweitzer *et al.* 1998).

The overall significance of such modulation is not known, but changes in SOM immunoreactivity and in morphology of SOM-positive neurones in the neocortex is a well recognized neurochemical indicator in late stage Alzheimer's disease (Armstrong *et al.* 1985). Whether this means that malfunction of MCs are involved in Alzheimer's disease is not clear because other morphological classes of interneurones (albeit less common) also express SOM. At the protein level, SOM was found to be expressed in wide arbour cells (Kawaguchi & Kubota, 1998). At the mRNA level, it was found to be expressed in small fractions of the small and nest basket cells, but hardly ever in large basket cells (Wang *et al.* 2002; Toledo-Rodriguez *et al.* 2003). SOM expression has also been detected in some bipolar, double bouquet and bitufted cells (Toledo-Rodriguez *et al.* 2003) (and authors' unpublished results).

All MCs lack the expression of PV and VIP. This is not due to false negatives, since the same technique reliably detected the expression of PV and VIP in other interneurone types (Wang *et al.* 2002; Toledo-Rodriguez *et al.* 2003, 2004). The finding is also in agreement with previous studies showing that at the protein level PV, VIP and SOM expression are found in different interneurones in

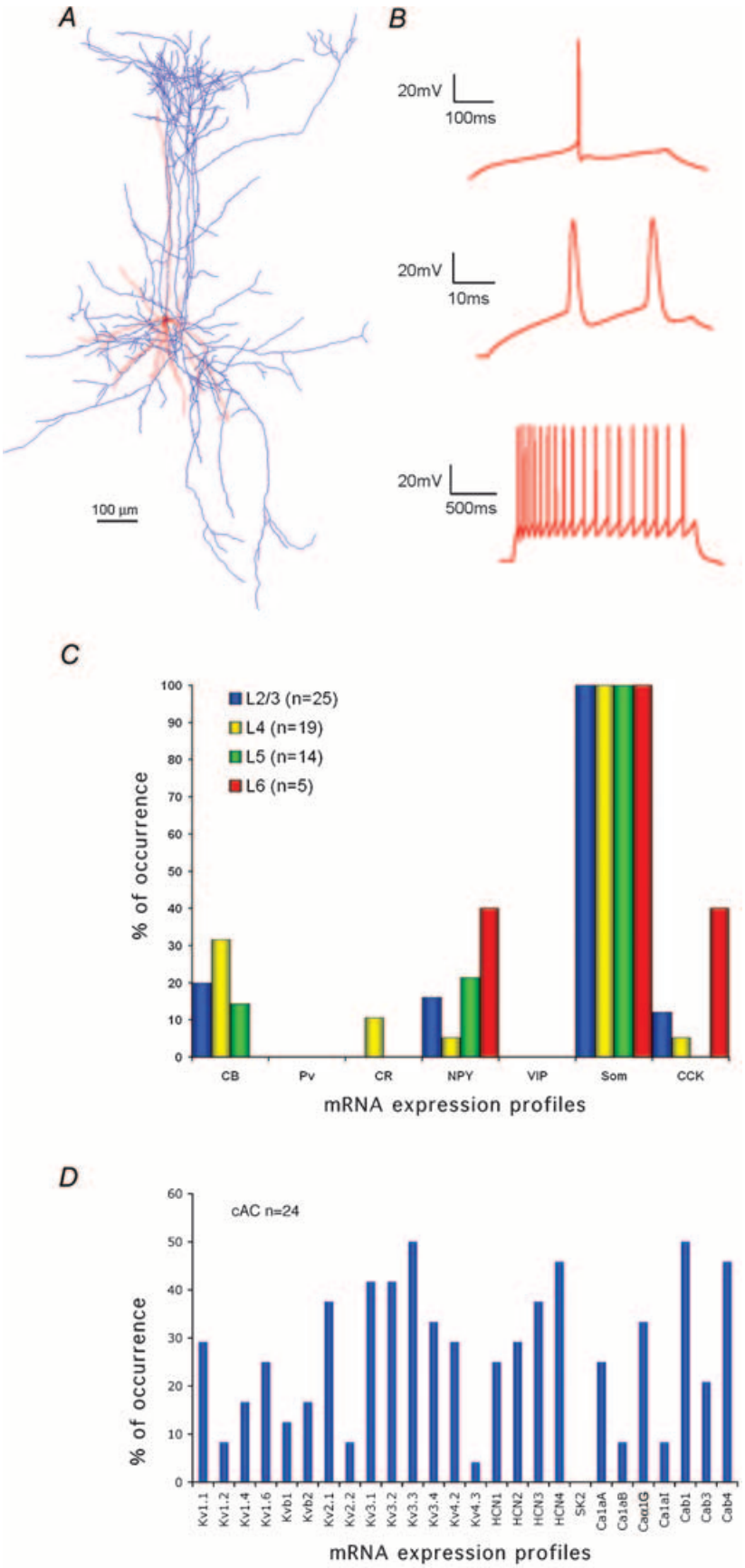

Figure 8. Gene expression in MCs
A, 3-D computer reconstruction. *B*, classical accommodation responses in a layer V MC. *C*, chart showing the percentage of MCs expressing different mRNAs encoding for the CaBPs (calbindin, CB; parvalbumin, PV; and calretinin, CR), neuropeptides (neuropeptide Y, NPY; vasoactive intestinal peptide, VIP; somatostatin, SOM; cholecystokinin, CCK) sorted according to layer. *D*, chart showing percentages of c-AC MCs expressing different mRNAs encoding for the voltage-activated K^+ channels (Kv1.1, Kv1.2, Kv1.4, Kv1.6, Kv2.1, Kv2.2, Kv3.1, Kv3.2, Kv3.3, Kv3.4, Kv4.2 and Kv4.3) and their auxiliary subunits (Kvβ1 and Kvβ2); the K^+/Na^+ permeable hyperpolarization-activated ion channels (HCN1, HCN2, HCN3 and HCN4) the Ca^{2+}-activated K^+ channel SK2; and the voltage-activated calcium channels (Caα1A, Caα1B, Caα1G and Caα1I) and their auxiliary subunits (Caβ1, Caβ3 and Caβ4).

layers II/III and IV of the rat frontal cortex (Kawaguchi & Kondo, 2002). SOM mRNA can, however, be co-expressed with VIP mRNA in bipolar, double-bouquet and small basket cells (Wang *et al.* 2002; Toledo-Rodriguez *et al.* 2003, 2004) (and authors' unpublished results), and regular spiking or irregular spiking cells (Cauli *et al.* 1997). At the mRNA level, a small percentage of interneurones co-express PV with SOM in large and nest basket cells (Wang *et al.* 2002), and fast spiking and regular spiking neurones (Cauli *et al.* 1997). A small basket cell also expressing SOM was found to co-express PV and VIP (Wang *et al.* 2002).

In addition to SOM, MCs also less frequently express other neuropeptides and calcium binding proteins, including CB, CR, NPY and CCK. These results confirm and extend previous findings (NPY expression (Beal *et al.* 1988; Kuljis & Rakic, 1989; Obst & Wahle, 1995); CB expression (Conde *et al.* 1994; Kawaguchi & Kubota, 1996, 1997; DeFelipe, 1997). These co-expressions could reflect molecular and functional heterogeneity of the MCs, but there is not sufficient data to make conclusive statements. Some trends are, however, worthy of further study. For example, the most common co-expression patterns were SOM–CB, SOM–NPY and SOM–CCK. CR expression was only detected in layer IV MCs, and CB was absent in layer IV MCs, which is consistent with the lack of burst-type MCs in layer IV. While the numbers are insufficient for a conclusive statement, it could be that CCK expression is absent from layer V MCs.

A multi-domain targeting interneurone

Interneurones differ in terms of their anatomical, electrophysiological and gene expression properties, and multiple attempts have been made to classify interneurones according to one or several of these properties. One scheme classifies interneurones according to the domain of the postsynaptic neurones targeted (Somogyi *et al.* 1982, 1998; Thomson & Deuchars, 1997; Toledo-Rodriguez *et al.* 2003). According to this scheme, there are four main classes of interneurones: those that inhibit the axon initial segment (e.g. axo-axonic or chandelier cells), those that inhibit the somatic and peri-somatic region (e.g. large, small and nest basket cells), those that inhibit the dendrites (e.g. bitufted cells, double bouquet cells, neurogliaform cells and bipolar cells), and those that target the most distal dendrites.

MCs target distal dendrites and therefore fall into the 4th class of distal dendritic targeting cells. However, MCs in all layers also arborize locally around their somata and EM analysis further revealed that while MCs innervate primarily dendrites of PCs, they can even innervate somata of PCs and dendritic shafts of interneurones, sharing some features of the 2nd and 3rd classes. This innervation overlaps with that of basket cells and suggests that MCs can also exert a classical fast local inhibitory feedback, more related to gain control than dendritic integration (Bernander *et al.* 1994; Mainen & Sejnowski, 1996). MCs can also innervate somata in layer I, which presumably belong to the rare layer I interneurones. These data therefore suggest that MCs have at least four different targeting strategies: (1) distal tuft dendrites of PCs in layer I, (2) apical and basal dendrites of PCs and interneurones, (3) somata of PCs, and (4) somata of interneurones in layer I.

A multi-layer and cross-columnar targeting interneurone

Layer I is an almost cell-free layer, which is scattered with a few rare cells such as the Cajal-Retzius cells. The somatic innervations found in layer I are presumably also onto these rare interneurones. Indeed, $GABA_A$ responses have been recorded in Cajal-Retzius cells (Radnikow *et al.* 2002). One possible function of such an innervation could be to modulate Cajal-Retzius cells, which releases reelin to guide PC positioning within the cortical column (Goh *et al.* 2002), suggesting that MCs may play an important role in development of the column.

The innervation of PC dendrites in layer I from neurones located in deeper layers is a specialized feature of MCs. These tufted dendrites have been shown to be essentially electrically separate compartments of the neurone (Yuste *et al.* 1994; Larkum *et al.* 1999, 2001) and the effect on dendritic integration is highly complex (Bernander *et al.* 1991; Larkum *et al.* 2001; Rhodes & Llinas, 2001). Layer I is a layer where the dendrites from PCs in all layers converge and inhibitory control of these tuft dendrites may be part of a cross-layer associational task. The main external input to layer I is also from the non-specific thalamus thought to be important in high level association tasks (Marin-Padilla, 1984). The horizontal layer I arborization to surrounding columns further suggests that the layer association task performed in layer I is co-ordinated with activity in neighbouring columns.

Layer II/III MCs heavily innervate layer I with less arborization around the somata. Layer II/III in general is more involved in cross-columnar and cross-region association (Jones *et al.* 1978; Lund *et al.* 1993; Kritzer & Goldman-Rakic, 1995), and the strong MC output to layer I to influence cross-layer association – a late stage in columnar processing. Layer II/III MCs also target their own layer, which is the primary target for spiny stellate excitation (Lübke *et al.* 2000) influencing a very early stage of columnar processing. Layer II/III MCs can therefore influence early and late stage columnar processing.

Layer IV MCs are characterized by their local dendritic and axonal expansions, indicating that they receive inputs from and distribute outputs mainly around their soma region. This localized morphology, like other types of

layer IV neurones (Lübke *et al.* 2000), may provide a direct negative feedback to layer IV, which is the main input layer from the specific thalamic nuclei (LeVay & Gilbert, 1976; White, 1989). Layer IV MCs provide only a comparatively minor output to layer I.

The axonal arborization of layer V and VI MCs suggests that these MCs are involved in multiple aspects of columnar processing. We show that a major target of MC axons from deep layers is layer IV. To our knowledge this specific targeting of layer IV has not been reported before. Layer V PCs are at the end stage of columnar processing providing the output to subcortical regions (see Sherman & Guillery, 2002). Thus, at the same time that information is transmitted out of the neocortex, layer V MCs provide negative feedback to the same layer, to the main input layer from the specific thalamus and to the main input layer from the non-specific thalamus. Layer V MCs may therefore be part of a negative feedback loop in the cortical column to inhibit incoming inputs during the output and/or to reset the column.

The axonal arborization of layer VI MCs is similar to that of layer V, but with a greater focus also on layer VI. Layer VI is the primary layer providing output to the specific thalamus (Gilbert & Kelly, 1975). While the main part of thalamic input enters at the level of layer IV, a significant fraction also enters directly into layer VI (Tömböl *et al.* 1976; Sherman & Guillery, 2002) and layer VI is therefore in a positive feedback loop with the same thalamic nucleus. This suggests that as layer VI PCs become activated, they would both activate specific thalamic neurones and, via the layer VI MCs, inhibit processing of specific thalamic input in layers IV and VI as well as processing of non-specific thalamic input in layer I. Layer VI MCs may therefore serve to prevent an explosive positive feedback with thalamus and/or may be part of a 'search-light type' selection–elimination iteration with the thalamus.

In summary, the axonal arborizations of MCs suggest that these interneurones control local processing in each neocortical layer and specifically target layer IV and layer I. MCs are therefore involved in iso-layer, cross-layer and cross-columnar negative feedback loops. It is tempting to speculate that MCs are involved in iterative fine tuning of the microcircuit activity due to input from association, columnar, thalamic and output to cortical, thalamic, sub-cortical regions.

Conclusion

This study reveals that MCs are a major type of interneurone in all layers II–VI of the rat somatosensory cortex. MCs are found to display common as well as layer-specific morphological, electrophysiological and biochemical properties. All MCs are multidomain targeting interneurones that enable multiple inhibitory feedback loops within each layer, from all cell layers II–VI to layer I, and from infragranular layers to layer IV. All MCs are also cross-columnar inhibitory interneurones via their horizontal axonal projection in layer I. MCs therefore seem to be involved in co-ordinating activity between layers and columns, in particular to control the gain of columnar activity within all layers, to provide negative feedback against sensory input from the specific and non-specific thalamus, against sensory association tasks from distant cortical regions, and against microcircuit activity when information flows out of the neocortex to subcortical regions. Many of these properties are likely to also hold in adult animals (see Introduction); for example, the characteristic morphology (bitufted), electrical behaviour (accommodating responses), and biochemical properties (SOM expression) are features also found in the adult neocortex.

References

Armstrong DM, LeRoy S, Shields D & Terry RD (1985). Somatostatin-like immunoreactivity within neuritic plaques. *Brain Res* **338**, 71–79.

Beal MF, Clevens RA & Mazurek MF (1988). Somatostatin and neuropeptide Y immunoreactivity in Parkinson's disease dementia with Alzheimer's changes. *Synapse* **2**, 463–467.

Bernander O, Douglas RJ, Martin KA & Koch C (1991). Synaptic background activity influences spatiotemporal integration in single pyramidal cells. *Proc Natl Acad Sci U S A* **88**, 11569–11573.

Bernander O, Koch C & Douglas RJ (1994). Amplification and linearization of distal synaptic input to cortical pyramidal cells. *J Neurophysiol* **72**, 2743–2753.

Cauli B, Audinat E, Lambolez B, Angulo MC, Ropert N, Tsuzuki K, Hestrin S & Rossier J (1997). Molecular and physiological diversity of cortical non pyramidal cells. *J Neurosci* **17**, 3894–3906.

Conde F, Lund JS, Jacobowitz DM, Baimbridge KG & Lewis DA (1994). Local circuit neurons immunoreactive for calretinin, calbindin D-28k or parvalbumin in monkey prefrontal cortex: distribution and morphology. *J Comp Neurol* **341**, 95–116.

De la Pena E & Geijo-Barrientos E (1996). Laminar localization, morphology, and physiological properties of pyramidal neurons that have the low-threshold calcium current in the guinea-pig medial frontal cortex. *J Neurosci* **16**, 5301–5311.

DeFelipe J (1997). Types of neurons, synaptic connections and chemical characteristics of cells immunoreactive for calbindin-D28K, parvalbumin and calretinin in the neocortex. *J Chem Neuroanat* **14**, 1–19.

Eccles JC (1983). The horizontal (tangential) fibres system of lamina I of the cerebral neocortex. *Acta Morph Hung* **31**, 261–284.

Fairen A, DeFelipe J & Regidor J (1984). Nonpyramidal neurons. In *Cerebral Cortex: Cellular Components of the Cerebral Cortex*, ed. Peters A & Jones E G, pp. 206–211. New York. Plenum Press.

Ferrer I, Fabregues I & Condom E (1986*a*). A Golgi study of the sixth layer of the cerebral cortex. I. The lissencephalic brain of Rodentia, Lagomorpha, Insectivora and Chiroptera. *J Anat* **145**, 217–234.

Ferrer I, Fabregues I & Condom E (1986*b*). A Golgi study of the sixth layer of the cerebral cortex. II. The gyrencephalic brain of Carnivora, Artiodactyla and Primates. *J Anat* **146**, 87–104.

Gabbott PL & Bacon SJ (1996). Local circuit neurons in the medial prefrontal cortex (areas 24a,b,c, 25 and 32) in the monkey. I. Cell morphology and morphometrics. *J Comp Neurol* **364**, 567–608.

Gilbert CD & Kelly JP (1975). The projections of cells in different layers of the cat's visual cortex. *J Comp Neurol* **163**, 81–105.

Goh KL, Cai L, Cepko CL & Gertler FB (2002). Ena/VASP proteins regulate cortical neuronal positioning. *Curr Biol* **12**, 565–569.

Goldberg JH, Lacefield CO & Yuste R (2004). Global dendritic calcium spikes in mouse layer 5 low threshold spiking interneurones: implications for control of pyramidal cell bursting. *J Physiol* **558**, 465–478.

Gupta A, Wang Y & Markram H (2000). Organizing principles for a diversity of GABAergic interneurones and synapses in the neocortex. *Science* **287**, 273–278.

Hedlich A & Werner L (1986). Classification of neurons of the visual cortex of the guinea pig (Cavia porcellus). A Golgi study. *J Hirnforsch* **27**, 651–677.

Hedlich A & Werner L (1990). Characteristics of neurons with intracortical axons spreading to the visual cortex of Alticola stoliczkanus barakshin and Alticola argentatus semicanus. A Golgi investigation. *J Hirnforsch* **31**, 779–787.

Hilbig H, Stubbe A & Winkelmann E (1991). Neurons in the visual cortex of Microtus brandti. *J Hirnforsch* **32**, 283–288.

Hubel DH & Wiesel TN (1962). Receptive fields, binocular interaction and functional architecture in the cat's visual cortex. *J Physiol* **160**, 106–154.

Lorente de No R (1938). Cerebral cortex: architecture, intracortical connections, motor projections. In: Physiology of the nervous system, 1st edition, ed. Fulton JF, pp. 291–329. Oxford University Press, New York.

Jones EG, Coulter JD & Hendry SH (1978). Intracortical connectivity of architectonic fields in the somatic sensory, motor and parietal cortex of monkeys. *J Comp Neurol* **181**, 291–347.

Kawaguchi Y (1995). Physiological subgroups of nonpyramidal cells with specific morphological characteristics in layer II/III of rat frontal cortex. *J Neurosci* **15**, 2638–2655.

Kawaguchi Y & Kondo S (2002). Parvalbumin, somatostatin and cholecystokinin as chemical markers for specific GABAergic interneuron types in the rat frontal cortex. *J Neurocytol* **31**, 277–287.

Kawaguchi Y & Kubota Y (1993). Correlation of physiological subgroupings of nonpyramidal cells with parvalbumin- and calbindinD28k-immunoreactive neurons in layer V of rat frontal cortex. *J Neurophysiol* **70**, 387–396.

Kawaguchi Y & Kubota Y (1996). Physiological and morphological identification of somatostatin- or vasoactive intestinal polypeptide-containing cells among GABAergic cell subtypes in rat frontal cortex. *J Neurosci* **16**, 2701–2715.

Kawaguchi Y & Kubota Y (1997). GABAergic cell subtypes and their synaptic connections in rat frontal cortex. *Cereb Cortex* **7**, 476–486.

Kawaguchi Y & Kubota Y (1998). Neurochemical features and synaptic connections of large physiologically-identified GABAergic cells in the rat frontal cortex. *Neuroscience* **85**, 677–701.

Kritzer MF & Goldman-Rakic PS (1995). Intrinsic circuit organization of the major layers and sublayers of the dorsolateral prefrontal cortex in the rhesus monkey. *J Comp Neurol* **359**, 131–143.

Kuljis RO & Rakic P (1989). Multiple types of neuropeptide Y-containing neurons in primate neocortex. *J Comp Neurol* **280**, 393–409.

Larkum ME, Zhu JJ & Sakmann B (1999). A new cellular mechanism for coupling inputs arriving at different cortical layers. *Nature* **398**, 338–341.

Larkum ME, Zhu JJ & Sakmann B (2001). Dendritic mechanisms underlying the coupling of the dendritic with the axonal action potential initiation zone of adult rat layer 5 pyramidal neurons. *J Physiol* **533**, 447–466.

LeVay S & Gilbert CD (1976). Laminar patterns of geniculocortical projection in the cat. *Brain Res* **113**, 1–19.

Lorente de No R (1922). La corteza cerebral del raton (Primera controbucion-la corteza acustica). *Trab Laboratory Invest Biol Madrid* **20**, 41–78.

Lübke J, Egger V, Sakmann B & Feldmeyer D (2000). Columnar organization of dendrites and axons of single and synaptically coupled excitatory spiny neurons in layer 4 of the rat barrel cortex. *J Neurosci* **20**, 5300–5311.

Lund JS, Yoshioka T & Levitt JB (1993). Comparison of intrinsic connectivity in different areas of macaque monkey cerebral cortex. *Cereb Cortex* **3**, 148–162.

Luth HJ, Hedlich A, Hilbig H, Winkelmann E & Mayer B (1994). Morphological analyses of NADPH-diaphorase/nitric oxide synthase positive structures in human visual cortex. *J Neurocytol* **23**, 770–782.

Mainen ZF & Sejnowski TJ (1996). Influence of dendritic structure on firing pattern in model neocortical neurons. *Nature* **382**, 363–366.

Marin-Padilla M (1970). Prenatal and early postnatal ontogenesis of the human motor cortex: a Golgi study. I. The sequential development of the cortical layers. *Brain Res* **23**, 167–183.

Marin-Padilla M (1972). Prenatal ontogenetic history of the principle neurons of the neocortex of the cat (Felis domestica): a Golgi study. II. Developmental differences and their significances. *Z Anat Entwicklungsgesch* **136**, 125–142.

Marin-Padilla M (1984). Neurons of layer I: a developmental analysis. In *Cerebral Cortex: Cellular Components of the Cerebral Cortex*, ed. Peters A & Jones E G, pp. 447–478. Plenum Press, New York.

Martinotti C (1889). Contributo allo studio della corteccia cerebrale, ed all'origine central dei nervi. *Ann Freniatr Sci Affini* **1**, 14–381.

Mountcastle VB (1957). Modality and topographic properties of single neurons in a cat's somatosensory cortex. *J Neurophysiol* **20**, 408–434.

O'Leary JL (1941). Structure of the area striata of the cat. *J Comp Neurol* **75**, 131–164.

Obst K & Wahle P (1995). Areal differences of NPY mRNA-expressing neurons are established in the late postnatal rat visual cortex in vivo, but not in organotypic cultures. *Eur J Neurosci* **7**, 2139–2158.

Peters A, Palay SL & Webster HD (1991). *The Fine Structure of the Nervous System: Neurons and Their Supporting Cells*. Oxford University Press, New York.

Porter JT, Cauli B, Tsuzuki K, Lambolez B, Rossier J & Audinat E (1999). Selective excitation of subtypes of neocortical interneurons by nicotinic receptors. *J Neurosci* **19**, 5228–5235.

Radnikow G, Feldmeyer D & Übke J (2002). Axonal projection, input and output synapses, and synaptic physiology of Cajal-Retzius cells in the developing rat neocortex. *J Neurosci* **22**, 6908–6919.

Ramon y Cajal S (1891). Sur la structure de l'ecorce cerebrale de quelques mammiferes. *Cellule* **7**, 3–54.

Ramon y Cajal S (1911). Histologie de systeme nerveux de 1 Homme et des vertebres tomme II (Paris, Maloine).

Rhodes PA & Llinas RR (2001). Apical tuft input efficacy in layer 5 pyramidal cells from rat visual cortex. *J Physiol* **536**, 167–187.

Ruiz-Marcos A & Valverde F (1970). Dynamic architecture of the visual cortex. *Brain Res* **19**, 25–39.

Schweitzer P, Madamba SG & Siggins GR (1998). Somatostatin increases a voltage-insensitive K^+ conductance in rat CA1 hippocampal neurons. *J Neurophysiol* **79**, 1230–1238.

Sherman SM & Guillery RW (2002). The role of the thalamus in the flow of information to the cortex. *Philos Trans R Soc Lond B Biol Sci* **357**, 1695–1708.

Shkol'nik-Yarros EG (1971). *Neurons and Interneuronal Connections of the Central Visual System*. Plenum Press, New York.

Simons DJ (1978). Response properties of vibrissa units in rat SI somatosensory neocortex. *J Neurophysiol* **41**, 798–820.

Somogyi P, Freund TF & Cowey A (1982). The axo-axonic interneuron in the cerebral cortex of the rat, cat and monkey. *Neuroscience* **7**, 2577–2607.

Somogyi P, Tamas G, Lujan R & Buhl EH (1998). Salient features of synaptic organisation in the cerebral cortex. *Brain Res Brain Res Rev* **26**, 113–135.

Staiger JF, Zilles K & Freund TF (1996). Recurrent axon collaterals of corticothalamic projection neurons in rat primary somatosensory cortex contribute to excitatory and inhibitory feedback-loops. *Anat Embryol* **194** (6), 533–543.

Swadlow HA (1989). Efferent neurons and suspected interneurones in S-1 vibrissa cortex of the awake rabbit: receptive fields and axonal properties. *J Neurophysiol* **62**, 288–308.

Tallent M & Siggins G (1997). Somatostatin depresses excitatory but not inhibitory neurotransmission in rat CA1 hippocampus. *J Neurophysiol* **78**, 3008–3018.

Thomson AM & Deuchars J (1997). Synaptic interactions neocortical local circuits: dual intracellular recordings *in vitro*. *Cereb Cortex* **7**, 510–522.

Toledo-Rodriguez M, Blumenfeld B, Wu C, Luo J, Attali B, Goodman P & Markram H (2004). Correlation maps allow neuronal electrical properties to be predicted from single-cell gene expression profiles in rat neocortex. *Cereb Cortex* **14**, 1310–1327.

Toledo-Rodriguez M, Gupta A, Wang Y, Wu CZ & Markram H (2003). Neocortex: basic neuron types. In *The Handbook of Brain Theory and Neural Networks*, ed. Arbib M A. MIT Press, Cambridge.

Tömböl T, Madaraz M, Hajdu F & Somogyi G (1976). Some data on the Golgi architecture of visual areas and suprasylvian gyrus in the cat. *Verh Anat Ges* **70**, 271–275.

Tommerdahl M, Favorov O, Whitsel BL, Nakhle B & Gonchar YA (1993). Minicolumnar activation patterns in cat and monkey SI cortex. *Cereb Cortex* **3**, 399–411.

Valverde F (1976). Aspects of cortical organization related to the geometry of neurons with intra-cortical axons. *J Neurocytol* **5**, 509–529.

Vogt BA & Peters A (1981). Form and distribution of neurons in rat cingulate cortex: Areas 32, 24, and 29. *J Comp Neurol* **195**, 603–625.

Wahle P (1993). Differential regulation of substance P and somatostatin in Martinotti cells of the developing cat visual cortex. *J Comp Neurol* **329**, 519–538.

Wang Y, Gupta A, Toledo-Rodriguez M, Wu CZ & Markram H (2002). Anatomical, physiological, molecular and circuit properties of nest basket cells in the developing somatosensory cortex. *Cereb Cortex* **12**, 395–410.

White EL (1989). Cortical circuits. In *Synaptic Organization of the Cerebral Cortex*. Birkhäuser, Boston.

Yamamoto T, Samejima A & Oka H (1988). Short latency activation of local circuit neurons in the cat somatosensory cortex. *Brain Res* **461**, 199–203.

Yuste R, Gutnick MJ, Saar D, Delaney KR & Tank DW (1994). Ca^{2+} accumulations in dendrites of neocortical pyramidal neurons: an apical band and evidence for two functional compartments. *Neuron* **13**, 23–43.